

Constraints on ion vs. electron heating by plasma turbulence at low beta

A. A. Schekochihin,^{1,2,3}† Y. Kawazura,¹‡ and M. A. Barnes^{1,4,5}

¹Rudolf Peierls Centre for Theoretical Physics, University of Oxford, Clarendon Laboratory, Parks Road, Oxford OX1 3PU, UK

²Merton College, Oxford OX1 4JD, UK

³Niels Bohr International Academy, Blegdamsvej 17, 2100 Copenhagen, Denmark

⁴University College, Oxford OX1 4BH, UK

⁵United Kingdom Atomic Energy Authority, Culham Science Centre, Abingdon OX14 3DB, UK

(compiled on 24 January 2022)

It is shown that in low-beta, weakly collisional plasmas, such as the solar corona, some instances of the solar wind, the aurora, inner regions of accretion discs, their coronae, and some laboratory plasmas, Alfvénic fluctuations produce no ion heating within the gyrokinetic approximation, i.e., as long as their amplitudes (at the Larmor scale) are small and their frequencies stay below the ion Larmor frequency (even as their spatial scales can be above or below the ion Larmor scale). Thus, all low-frequency ion heating in such plasmas is due to compressive fluctuations (“slow modes”): density perturbations and non-Maxwellian perturbations of the ion distribution function. Because these fluctuations energetically decouple from the Alfvénic ones already in the inertial range, the above conclusion means that the energy partition between ions and electrons in low-beta plasmas is decided at the outer scale, where turbulence is launched, and can be determined from magnetohydrodynamic (MHD) models of the relevant astrophysical systems. Any additional ion heating must come from non-gyrokinetic mechanisms such as cyclotron heating or the stochastic heating owing to distortions of ions’ Larmor orbits. An exception to these conclusions occurs in the Hall limit, i.e., when the ratio of the ion to electron temperatures is as low as the ion beta (equivalently, the electron beta is order unity). In this regime, slow modes couple to Alfvénic ones well above the Larmor scale (viz., at the ion inertial or ion sound scale), so the Alfvénic and compressive cascades join and then separate again into two cascades of fluctuations that linearly resemble kinetic Alfvén and ion cyclotron waves, with the former heating electrons and the latter ions. The two cascades are shown to decouple, scalings for them are derived, and it is argued physically that the two species will be heated by them at approximately equal rates.

1. Introduction

One of the most fundamental questions in plasma astrophysics is what determines the temperatures of different particle species, ions (T_i) and electrons (T_e). We know that a system with different T_i and T_e is not in equilibrium and so must have an intrinsic (although not necessarily overwhelming) tendency to relax to an equi-temperature state. We do not, however, know of any mechanisms other than Coulomb collisions that

† Email: alex.schekochihin@physics.ox.ac.uk

‡ New address: Frontier Research Institute for Interdisciplinary Sciences and Department of Geophysics, Tohoku University, Aramaki aza Aoba 6-3, Aoba-ku, Sendai 980-8578, Japan.

would equalise the temperatures. There are no instabilities of a spatially homogeneous equilibrium with $T_i \neq T_e$ Maxwellian ions and electrons and so there is no obvious way in which, e.g., turbulence could result and quickly equalise the temperatures. In the absence of such fast dynamical processes, collisions are all that remains. In a large class of astrophysical and space plasmas where collisions are not very frequent, temperature equalisation by collisions is extremely slow: the relevant collision frequency is the ion–electron one, ν_{ie} , which is a factor of mass ratio, m_e/m_i , smaller even than the electron collision frequency and a factor of $(m_e/m_i)^{1/2}$ smaller than the ion one. This means that, for most practical purposes, an “incomplete” equilibrium with $T_i \neq T_e$ must be assumed (e.g., [Braginskii 1965](#))—and that is indeed what is observed in the solar wind (see, e.g., [Cranmer *et al.* 2009](#), and references therein). It is not, however, known what determines the ratio T_i/T_e —a question that is also of great interest in the context of extragalactic plasmas, e.g., accretion discs, where only T_e is measured, but knowledge of T_i is required for the understanding of basic plasma processes and model building (e.g., [Quataert 2003](#); [Sharma *et al.* 2007](#); [Ressler *et al.* 2017](#); [Rowan *et al.* 2017, 2019](#); [Chael *et al.* 2018*b,a*](#); [Chandran *et al.* 2018](#)).

Collisions aside, T_i and T_e can be changed via heating or cooling processes resulting from energy exchange between the mean (equilibrium) particle distributions and fluctuations (or waves), which are ubiquitously present in space and astrophysical plasmas—while temperature difference does not drive fluctuations, there are plenty of free-energy sources that do (background gradients, large-scale stirring, etc.). The free energy of these fluctuations is processed through phase space by various nonlinear (e.g., turbulence) and linear (e.g., phase mixing) mechanisms, brought to suitably small scales and thermalised, giving rise to ion or electron heating (see, e.g., [Schekochihin *et al.* 2008, 2009, 2016](#); [Kawazura *et al.* 2019](#); [Meyrand *et al.* 2019](#)). The interesting question then is what fraction of the free energy injected at large scales is deposited into the thermal energy of each species.

Much of the turbulence actually observed or theoretically expected in magnetised astrophysical plasmas is in the form of low-frequency, magnetohydrodynamic (MHD)-scale Alfvénic or compressive (“slow-mode”) fluctuations. They are at low frequencies because they are typically excited by large-scale mechanisms and because their cascade to smaller scales is anisotropic with respect to their local magnetic field, $k_{\parallel} \ll k_{\perp}$, implying that the Larmor scales (ρ_i, ρ_e) in the perpendicular direction are reached before the Larmor frequencies (Ω_i, Ω_e) (see [Schekochihin *et al.* 2009](#), and references therein; this paper is henceforth referred to as S09). Thus, opportunities for transferring the energy of the turbulent cascade into ion thermal energy via the Landau damping of compressive fluctuations (throughout the inertial range; see S09–§6 and [Meyrand *et al.* 2019](#)) or via the ion entropy cascade (starting at the ion Larmor scale; see S09–§7 and [Kawazura *et al.* 2019](#)) occur before (i.e., at larger scales than) the cyclotron heating can take place ([Howes *et al.* 2008*a*](#)). All of these low-frequency heating routes can be treated in the so-called gyrokinetic (GK) approximation ([Frieman & Chen 1982](#); [Howes *et al.* 2006](#), the latter paper is henceforth referred to as H06). This has the twin advantages of greater analytical tractability than the full Vlasov–Maxwell kinetics and very much greater feasibility of three-dimensional (3D) direct numerical simulations ([Howes *et al.* 2008*b*, 2011](#); [TenBarge *et al.* 2013](#); [Told *et al.* 2015](#); [Bañón Navarro *et al.* 2016](#); [Li *et al.* 2016](#); [Kawazura *et al.* 2019](#)).¹ The goal of such analytical and numerical inquiries is to

¹3D is the only relevant kind of simulations in this context because only in 3D can both the dominant nonlinearity and wave propagation be captured simultaneously (see, e.g., [Howes 2015](#)). It is only in the last year that 3D full-Vlasov-kinetic simulations of the problem have

parametrise ion and electron heating in terms of the two main plasma parameters, T_i/T_e and plasma beta, the latter defined to be the ratio of the ion thermal and magnetic energies, $\beta_i = 8\pi n_i T_i / B^2$ (where n_i is the ion density and B is the magnetic field).

Analytically, determining ion heating in anything like a definitive fashion has so far turned out to be a rather difficult task, except in the linear approximation (Quataert 1998; Quataert & Gruzinov 1999). While progress can be made via modeling based on physically reasonable conjectures (e.g., Breech *et al.* 2009; Chandran *et al.* 2009, 2010; Chandran 2010; Howes 2010, 2011), it is very useful to have some non-negotiable constraints on the answer, valid under clearly stated assumptions, such as the GK regime adopted here. In this paper, we show that it is possible to establish such constraints in a fairly straightforward way for low-beta plasmas, a subset that, while very far from being exhaustive, does include some observationally accessible cases, e.g., the solar corona (Aschwanden *et al.* 2001; Cranmer 2009), some episodes of the solar wind at 1 AU (Smith *et al.* 2001), the aurora (Chaston *et al.* 2008), maybe, in the near future, certain regions of accretion discs (Chael *et al.* 2018*b,a*), and, finally, laboratory plasmas such as the LAPD, custom-made for studies of Alfvén waves (Carter *et al.* 2006; Gekelman *et al.* 2011).

In what follows, we will first, in section 2, give a qualitative physical outline of our argument and its implications. A reader uninterested in theoretical rigour need not read anything else. The subsequent three sections are dedicated to providing a systematic calculation to back up the statements made in section 2. Section 3 is a quick recapitulation of the GK formalism needed in what follows. Section 4 contains the derivation of a reduced set of equations satisfied by plasma turbulence in the low-beta limit and the proof, based on those equations, that, in low-beta plasmas, there is no ion heating due to Alfvénic fluctuations and that all ion heating that does occur is due to compressive fluctuations found in the inertial range. Section 5 (whose length is perhaps incommensurate with its importance in the grand scheme of things) deals with a particular type of low-beta plasma where ions are much colder than electrons (the “Hall limit”), where it turns out that the conclusion of section 4 must be substantially revised and the ion and electron heating rates are likely to be comparable (on the way, some conceptually interesting results on Hall turbulence emerge: see section 5.5). Finally, in section 6, there is a brief closing discussion, in particular of possible self-regulation mechanisms for ion heating.

2. Epitome

When turbulence in a plasma is stirred up by some large-scale mechanism, this amounts to ion and electron distribution functions being perturbed away from equilibrium. If these perturbations are low-frequency ($\omega \ll \Omega_i$) and large-scale ($k\rho_i \ll 1$, where ρ_i is the ion Larmor radius), they will, via nonlinear interactions, generate further, smaller-amplitude, smaller-scale, higher-frequency fluctuations. Just as in ordinary fluid turbulence, this process can be conceptualised as a cascade of energy—in the case of kinetic (collisionless or weakly collisional) plasma, a cascade of free energy associated with the perturbed distribution functions and electromagnetic fields (see Schekochihin *et al.* 2008 and references therein). In the presence of a strong magnetic field, the fluctuations produced by this cascade are expected—and, indeed, observed, in numerical simulations (Cho & Vishniac 2000; Maron & Goldreich 2001) and in the solar wind (Horbury *et al.*

become possible (Cerri *et al.* 2018; Grošelj *et al.* 2018; Franci *et al.* 2018; Arzamasskiy *et al.* 2019; Zhdankin *et al.* 2019).

2008; Podesta 2009; Wicks *et al.* 2010; Chen *et al.* 2011; Chen 2016)—to be ever more scale-anisotropic at ever smaller scales, viz., long along the field, short across it: $k_{\parallel} \ll k_{\perp}$.

In this anisotropic limit, the fluctuations at scales greater than ρ_i can be classified into two kinds:

(i) *Alfvénic*, i.e., incompressible perpendicular MHD perturbations of the velocity and magnetic field, \mathbf{u}_{\perp} and \mathbf{b}_{\perp} —these correspond to Maxwellian perturbations of the ion distribution function with flow velocity $\mathbf{u}_{\perp} = c\mathbf{E} \times \mathbf{B}_0/B_0^2$, where \mathbf{E} is the perturbed electric field and \mathbf{B}_0 the mean magnetic field (see S09–§5);

(ii) *compressive*, i.e., perturbations of plasma density δn_e ($= \delta n_i n_e/n_i$ by quasineutrality), field strength δB , and general perturbations of the ion distribution function involving parallel flow velocity, temperature and higher moments (see S09–§6); these perturbations are the kinetic version of the MHD slow modes.²

It is then possible to prove (S09–§5, 6), for any β_i and T_i/T_e and assuming that the equilibrium distribution function is either Maxwellian or satisfies certain constraints (Kunz *et al.* 2015), that these two types of fluctuations are energetically decoupled from each other: the cascade of the free energy splits into an MHD “Alfvén-wave cascade” and a cascade of compressive fluctuations, passively advected by the Alfvén-wave turbulence but unable to exchange energy with it. In a weakly collisional plasma, i.e., one in which collision rates are small compared to the characteristic frequencies of the turbulent fluctuations, the latter cascade is potentially subject to Landau–Barnes damping (Barnes 1966), which will give rise to (parallel) ion heating at all scales in the “inertial range” ($k_{\perp}\rho_i < 1$). However, the nonlinear cascade rate is comparable to the Alfvén frequency, $k_{\parallel}v_A$, where $v_A = B_0/\sqrt{4\pi m_i n_i}$ is the Alfvén speed (Goldreich & Sridhar 1995, 1997), whereas the damping rate cannot be much larger than $\sim k_{\parallel}v_{\text{th}i}$, where $v_{\text{th}i} = \sqrt{2T_i/m_i}$ is the ion thermal speed (S09–§6.2.2). In low-beta plasmas, $v_{\text{th}i} = \sqrt{2T_i/m_i} = \sqrt{\beta_i}v_A \ll v_A$, so the damping is expected to be negligible compared to the rate of nonlinear transfer of the fluctuation energy towards the Larmor scale³ (cf. Lithwick & Goldreich 2001).

This means that (in a weakly collisional plasma) no thermalisation of any of that energy can occur until the fluctuations have reached $k_{\perp}\rho_i \sim 1$. At this point, the free-energy cascade is, in general, no longer split into Alfvénic and compressive, the two types of fluctuations can couple and the free energy can be shown to be cleanly split again into two decoupled cascades only at $k_{\perp}\rho_i \gg 1$. These two sub-Larmor dissipation channels are the cascades of kinetic Alfvén waves (KAW) and of ion entropy (S09–§7; that the sub-Larmor-range turbulence in the solar wind is indeed predominantly of the KAW kind appears to be settled: see Salem *et al.* 2012, Chen *et al.* 2013, and the references in footnote 2). The KAW eventually thermalise into electrons, via Landau damping and/or

²High-frequency modes, such as fast magnetosonic waves (at inertial-range scales) or whistlers (at sub-ion-inertial scales), can be self-consistently ignored in the anisotropic regime that we are considering—and indeed are ordered out in the GK approximation (see H06–§2.2). This does not mean that they cannot exist, just that they can not-exist, i.e., that they would not be triggered by the motions and fields that are retained. Observations of solar-wind turbulence in the inertial range suggest that fast-wave energy is indeed negligible (Howes *et al.* 2012). Around the ion Larmor scale, an energetically subdominant population of non-GK perturbations, viz., whistler and ion-cyclotron waves with large k_{\parallel} , is observed in the solar wind (Wicks *et al.* 2010; Podesta & Gary 2011; He *et al.* 2011, 2012; Klein *et al.* 2014; Lion *et al.* 2016) and may be due to pressure-anisotropy instabilities, which are not captured by GK, but are not a significant danger at low beta (e.g., Hellinger *et al.* 2006; Bale *et al.* 2009; Kunz *et al.* 2018).

³Interestingly, it turns out that even at $\beta_i \sim 1$, Landau damping in the inertial range can be effectively suppressed by a nonlinear effect, the stochastic echo (Meyrand *et al.* 2019), and the compressive free energy cascades mostly unimpeded towards the Larmor scale.

via various dissipation effects at or below the electron Larmor scale.⁴ The ion entropy cascade is a nonlinear mixing process in phase space, resulting in fine-scale structure in the ion distribution function and eventually thermalised into ions by collisions—as large gradients in v_\perp form alongside large spatial gradients, even very low collisionality is enough to dissipate non-Maxwellian perturbations at a finite rate (S09–§§7.9 and 7.10).

Thus, how much energy goes into ions and how much into electrons is decided when the free-energy cascade reconstitutes itself and then splits again at the ion Larmor scale. Therefore, any analytical treatment of this problem requires a theoretical description uniformly valid for $k_\perp \rho_i$ small, large and order-unity. Gyrokinetics is such a theory, requiring low frequencies ($\omega \ll \Omega_i$) but not long wavelengths (see H06 for a tutorial). However, in its general form, it does not make the problem of energy partition between species any more analytically tractable (although it does make numerical simulations of this process more feasible: Howes *et al.* 2008b, 2011; TenBarge *et al.* 2013; Told *et al.* 2015; Bañón Navarro *et al.* 2016; Li *et al.* 2016; Kawazura *et al.* 2019, the latter paper being the closest that we have got to an actual solution of the problem, at least within the GK approximation).

A dramatic simplification occurs if β_i is assumed small. In this limit, $v_{\text{th}i}/v_A = \sqrt{\beta_i} \ll 1$, so ions cannot stream along the field lines fast enough to couple properly to the electromagnetic fields associated with the Alfvén waves, MHD or kinetic, and so perturbations of the ion distribution function (other than the Maxwellian $\mathbf{E} \times \mathbf{B}$ drift) stay decoupled from the Alfvénic cascade.⁵ As we shall demonstrate below, this makes it possible to prove that, in the low-beta limit, compressive perturbations of the ion distribution function will cascade from the inertial range, through the ion Larmor scale and turn into the ion entropy cascade at sub-Larmor scales and then into ion heat without exchanging any energy with the Alfvénic fluctuations. All of the energy of the latter turns into KAW energy, which includes density perturbations at sub-Larmor scales, but cascades separately from the ion entropy and is eventually dissipated on electrons. Proving this analytically is accomplished by showing that a certain form of the free-energy invariant,

⁴Because $k_\parallel \ll k_\perp$, the frequency of the turbulent fluctuations at $k_\perp \rho_i \sim 1$ is still much smaller than Ω_i . If the cyclotron frequency is reached by the KAW cascade at sub-Larmor scales, cyclotron heating can result, linearly, but the wave number range in which it occurs is quite narrow (see Appendix of Howes *et al.* 2008a) and it remains to be seen whether it would be effective at all in a nonlinear situation (see, however, Arzamasskiy *et al.* 2019). In any event, this heating mechanism is outside the scope of our treatment here; we acknowledge its possible contribution as a source of additional ion heating but remain agnostic about the amount of such heating.

⁵It is perhaps worth emphasising that it is the ion beta, β_i , that must be low, while β_e may or may not be (the possibility that it is not is covered by the Hall limit; see the end of this section and section 5). The regime in which $\beta_i \sim 1$ but $\beta_e \ll 1$, i.e., electrons are colder than ions, $ZT_e/T_i \ll 1$, is covered by the theory for order-unity or high β_i , which we do not attempt here (for a numerical study of what happens there, see Kawazura *et al.* 2019). The only difference between this regime and $\beta_e \sim \beta_i \sim 1$ is that, since $d_e = \rho_e/\sqrt{\beta_e} \gg \rho_e$, the electron inertial effects come in before the KAW cascade reaches the electron Larmor scale. This modifies the structure of the KAW cascade (Chen & Boldyrev 2017; Passot *et al.* 2017), but should not change the fact that all the energy that is processed through it goes into electrons. Such a physical situation is observable in the Earth’s magnetosheath (Chen & Boldyrev 2017). Interesting changes in the energy partition may be possible if β_e is so low that $d_e \gtrsim \rho_i$, even though $\beta_i \sim 1$. This is possible if $ZT_e/T_i \sim \beta_e \sim m_e/m_i$, perhaps too extreme a limit. We shall not consider it here. Note that the case of $\beta_e \sim m_e/m_i$ and $\beta_i \ll 1$ (considered by Zocco & Schekochihin 2011 and easy to simulate; see Loureiro *et al.* 2013, 2016; Grošelj *et al.* 2017) is no different, as far as energy partition is concerned, from the standard low-beta regime—Alfvénic fluctuations heat electrons, compressive ones heat ions (see section 4.7).

which reduces to the energy of Alfvénic and KAW perturbations in the long- and short-wavelength limits, respectively, is conserved across the ion-Larmor-scale transition and thus no Alfvénic energy can leak into ion heat (see section 4). Therefore, only the energy of what started out as compressive cascade in the inertial range will contribute to ion heating, at least to the extent that the GK approximation holds. Any further ion heating will have to come from non-GK mechanisms such as cyclotron heating (Gary *et al.* 2005; Kasper *et al.* 2008, 2013; Marsch & Bourouaine 2011; Arzamasskiy *et al.* 2019) or stochastic orbit deformations (Chandran *et al.* 2010; Chandran 2010; Vech *et al.* 2017; Mallet *et al.* 2018; Arzamasskiy *et al.* 2019, see section 6.1).

The key “practical” (in astrophysics, this means relevant to large-scale modelling) conclusion from all this is that at low β_i , *the energy partition between ions and electrons is determined already at the outer scale of the MHD cascade*, where the energy flux splits into Alfvénic and compressive. Once this separation occurs, the ratio between ion and electron heating rates is fixed. Thus, what in principle is a microscale kinetic effect is in fact fully constrained by fluid dynamics.⁶ Since all the action is at the outer scale, the ion-to-electron heating ratio may depend on various nonuniversal circumstances, e.g., presence of equilibrium temperature stratification (which will produce temperature perturbations), shear, rotation, configuration of magnetic field, etc.

These conclusions hold provided $\beta_e \sim \beta_i \ll 1$. When $\beta_i \ll 1$ but $\beta_e \sim 1$, i.e., when ions are much colder than electrons, $ZT_e/T_i \gg 1$ (the so-called Hall limit; S09–§E), the situation changes substantially (section 5). The physical difference between the $ZT_e/T_i \sim 1$ and $ZT_e/T_i \gg 1$ cases is that in the latter limit, slow magnetoacoustic waves are faster than the ions (because both the Alfvén speed and the sound speed $c_s = \sqrt{ZT_e/m_i}$ are larger than v_{thi}), remain undamped, and join happily with the AW cascade at a certain transition scale that is larger than ρ_i [it is either the ion inertial or ion sound scale; see (5.19)]. At this transition scale, the Alfvénic and compressive cascades re-couple and, below the transition scale, turn into cascades of higher-frequency KAW (or, as they are sometimes called in the context of Hall MHD, whistlers) and lower-frequency oblique ion cyclotron waves (ICW). In section 5.5, we argue, with some support from numerical simulations (Meyrand *et al.* 2018), that the two cascades are energetically decoupled and critically balanced, enabling one to predict their scalings easily: the KAW scalings [see (5.47)] are the usual ones, as derived in S09–§7.5 and Cho & Lazarian (2004); the ICW scalings [see (5.52)] are the same as the scalings for the inertial-wave turbulence proposed by Nazarenko & Schekochihin (2011) (both sets of scalings can be related to some of the spectra previously posited by Krishan & Mahajan 2004 and by Galtier & Buchlin 2007, and seen numerically by Meyrand & Galtier 2012). It is then possible to prove rigorously that the KAW cascade will heat electrons and the ICW cascade will heat ions—because the latter turns into the ion-entropy cascade (S09–§7.10), whereas the former transitions through the ion Larmor scale without coupling to ions and turns into the sub-Larmor KAW cascade (this is all worked out in detail and further discussed in section 5.7). We also argue, on physical grounds rather than rigorously, that the partition of energy flowing into the two cascades and, therefore, into the two species, should be

⁶This is, of course, only true assuming that the outer scale is collisional, so the Alfvénic and compressive cascades split within the MHD approximation and the transition to collisionless regime occurs within the compressive cascade (see S09–§6). If the plasma is collisionless already at the outer scale, how the cascades separate is a fully kinetic problem, even if still a large-scale one. Furthermore, in such a plasma, if $\delta B/B \sim 1$ at the outer scale and beta is low, the fluctuation energy far exceeds the thermal energy and one can hardly assume that a two-temperature Maxwellian equilibrium would either be established or survive. We are not addressing here the “violent relaxation” of such situations.

approximately equal, independently of how much of the original MHD cascade is Alfvénic and how much compressive (section 5.5.4). Here again, the energy partition is decided at fluid scales, but at the Hall transition scale rather than at the outer scale.

The following sections are mostly technical in nature (except for sections 5.5.1, 5.5.2 and 5.5.4) and dedicated to proving the statements made above. In the process, we also derive a number of simple and appealing reduced models of various types of kinetic turbulence, which can be studied analytically and numerically using these models, either for its own sake or with some applied purpose. A reader uninterested in analytical detail can now skip to section 6.

3. Gyrokinetic Primer

This section is an extended recapitulation of the GK formalism that is required for subsequent developments. In principle, all of this is already available from H06 and S09 (and, in a form generalised to non-Maxwellian equilibria, from Kunz *et al.* 2015, 2018), but we provide this refreshed version for the convenience of the reader and as an opportunity to adjust notation, to deal with some subtleties, and to cast some of the derivations in what we now consider a more optimal form. A reader familiar with H06 and S09 may wish to skip (or skim) this section and then refer back to it as required during the reading of the rest of the paper.

3.1. Notation: Alfvénic Fields

The electric and magnetic fields are described by the scalar potential ϕ and vector potential \mathbf{A} . It is convenient to introduce dimensionless versions of ϕ and of the component of \mathbf{A} parallel to the equilibrium magnetic field $\mathbf{B}_0 = B_0 \hat{\mathbf{z}}$:

$$\varphi = \frac{Ze\phi}{T_i} = \frac{2\Phi}{\rho_i v_{\text{th}i}}, \quad \mathcal{A} = \frac{A_{\parallel}}{\rho_i B_0} = -\frac{\Psi}{\rho_i v_A}, \quad (3.1)$$

where $-e$ is the electron charge, Ze the ion charge, T_i the ion equilibrium temperature, $v_{\text{th}i} = \sqrt{2T_i/m_i}$ the ion thermal speed, m_i the ion mass, $\rho_i = v_{\text{th}i}/\Omega_i$ the ion Larmor radius, $\Omega_i = ZeB_0/m_i c$ the ion Larmor frequency, c the speed of light, $v_A = B_0/\sqrt{4\pi m_i n_i}$ the Alfvén speed, and n_i the equilibrium ion density. In what follows, we shall drop the ion species index everywhere except for some iconic quantities (e.g., ρ_i) or where there is a possibility of ambiguity (e.g., T_i vs. T_e).

In the above, we have also introduced the stream function $\Phi (= c\phi/B_0)$ of the $\mathbf{E} \times \mathbf{B}$ flow associated with ϕ and the flux function Ψ giving (in velocity units) the magnetic-field perturbation perpendicular to \mathbf{B}_0 :

$$\mathbf{u}_{\perp} = \hat{\mathbf{z}} \times \nabla_{\perp} \Phi, \quad \mathbf{b}_{\perp} = \hat{\mathbf{z}} \times \nabla_{\perp} \Psi. \quad (3.2)$$

Physically these perturbations are Alfvén waves (AW). In the inertial range of magnetised plasma turbulence, they decouple from all other modes (the fast modes, which are ordered out in the GK approximation, and the slow, or compressive, modes) and satisfy the “Reduced MHD” equations (RMHD, first derived by Kadomtsev & Pogutse 1974 and Strauss 1976; for a GK derivation, see S09–§5.3):

$$\frac{\partial \Psi}{\partial t} = v_A \nabla_{\parallel} \Phi, \quad \frac{d}{dt} \nabla_{\perp}^2 \Phi = v_A \nabla_{\parallel} \nabla_{\perp}^2 \Psi. \quad (3.3)$$

Here the nonlinearities are hidden in the convective time derivative and in the spatial

derivative along the perturbed field lines:

$$\frac{d}{dt} = \frac{\partial}{\partial t} + \mathbf{u}_\perp \cdot \nabla_\perp = \frac{\partial}{\partial t} + \{\Phi, \dots\} = \frac{\partial}{\partial t} + \frac{\rho_i v_{\text{th}i}}{2} \{\varphi, \dots\}, \quad (3.4)$$

$$\nabla_\parallel = \frac{\partial}{\partial z} + \frac{\mathbf{b}_\perp}{v_A} \cdot \nabla_\perp = \frac{\partial}{\partial z} + \frac{1}{v_A} \{\Psi, \dots\} = \frac{\partial}{\partial z} - \rho_i \{\mathcal{A}, \dots\}, \quad (3.5)$$

where $\{f, g\} = (\partial_x f)(\partial_y g) - (\partial_x g)(\partial_y f)$. These derivatives will appear ubiquitously in what follows.

3.2. Gyrokinetic Equation

Our starting point is standard, slab, Maxwellian gyrokinetics (see the derivation in H06 or a summary in S09–§3). In it, the ion distribution function is represented as

$$f = F_0 + \delta f, \quad \delta f = -\varphi(\mathbf{r})F_0 + h(\mathbf{R}), \quad \mathbf{R} = \mathbf{r} + \boldsymbol{\rho}, \quad \boldsymbol{\rho} = \frac{\mathbf{v}_\perp \times \hat{\mathbf{z}}}{\Omega}, \quad (3.6)$$

where \mathbf{R} is the GK spatial coordinate (centre of Larmor ring), whereas \mathbf{r} is the usual spatial coordinate (position of the particle). Then the GK equation for the evolution of h is

$$\frac{\partial h}{\partial t} + v_\parallel \frac{\partial h}{\partial z} + \frac{\rho_i v_{\text{th}}}{2} \{\langle \chi \rangle_{\mathbf{R}}, h\} = \frac{\partial \langle \chi \rangle_{\mathbf{R}}}{\partial t} F_0 + C[h] + \frac{2v_\parallel \langle a_{\text{ext}} \rangle_{\mathbf{R}}}{v_{\text{th}}^2} F_0. \quad (3.7)$$

Here the GK potential gyroaveraged at constant \mathbf{R} (an operation denoted by angle brackets) is

$$\langle \chi \rangle_{\mathbf{R}} = \frac{Ze}{T_i} \left\langle \phi - \frac{\mathbf{v} \cdot \mathbf{A}}{c} \right\rangle_{\mathbf{R}} = \hat{J}_0 \varphi - 2\hat{v}_\parallel \hat{J}_0 \mathcal{A} + \hat{v}_\perp^2 \hat{J}_1 \frac{\delta B}{B}, \quad (3.8)$$

where $\hat{v}_\parallel = v_\parallel/v_{\text{th}}$, $\hat{v}_\perp = v_\perp/v_{\text{th}}$, δB is the perturbation of the magnetic field along itself (related to \mathbf{A}_\perp), which is also the perturbation of the field's strength; the gyroaveraging Bessel operators are defined in terms of their Fourier space representations:

$$\hat{J}_0 \leftrightarrow J_0(a) = 1 - \frac{a^2}{4} + \dots, \quad \hat{J}_1 \leftrightarrow \frac{2J_1(a)}{a} = 1 - \frac{a^2}{8} + \dots, \quad a = \frac{k_\perp v_\perp}{\Omega} = \hat{v}_\perp k_\perp \rho_i. \quad (3.9)$$

Obviously, $a^2 \leftrightarrow -\hat{v}_\perp^2 \rho_i^2 \nabla_\perp^2 = -\hat{v}_\perp^2 \hat{\nabla}_\perp^2$, where we denote $\hat{\nabla}_\perp = \rho_i \nabla_\perp$. We shall use the \hat{J} notation (Kunz *et al.* 2018) interchangeably with $\langle \dots \rangle_{\mathbf{R}}$ (or with $\langle \dots \rangle_{\mathbf{r}}$, the gyroaverage of an \mathbf{R} -dependent quantity at constant \mathbf{r}), as proves convenient.

The last term in (3.7) represents energy injection by means of an external parallel acceleration a_{ext} . This will be a convenient model of the excitation of compressive perturbations for further calculations dealing with free-energy budgets. Finally, the collision operator $C[h]$ contains both the ion-ion and ion-electron collisions, but the latter are negligible in the mass-ratio expansion adopted below.

3.3. Isothermal Electron Fluid

We supplement the ion GK equation (3.7) with two fluid equations arising from the isothermal approximation for electrons, which is a result of expansion in the electron-ion mass ratio and holds at $k_\perp \rho_e \ll 1$,⁷ and with field equations that follow from quasineutrality and Ampère's law in the same approximation (this system of equations was derived

⁷This is as good a place as any to address a certain resentment that a reader with a predilection for mathematical rigour (e.g., Eyink 2015, 2018) might experience towards approximate equations valid in restricted scale subranges. Generally speaking, nonlinear solutions of such approximate equations will not stay within their own bounds of validity and develop gradients on scales that are smaller than allowed by the assumed ordering. This is, of course, what turbulence

in S09–§4, implemented numerically by [Kawazura & Barnes 2018](#) and simulated to some useful effect by [Kawazura *et al.* 2019](#)):

$$\frac{\partial \mathcal{A}}{\partial t} + \frac{v_{\text{th}}}{2} \nabla_{\parallel} \varphi = \frac{v_{\text{th}}}{2} \nabla_{\parallel} \frac{Z}{\tau} \frac{\delta n}{n} + \eta \nabla_{\perp}^2 \mathcal{A}, \quad (3.10)$$

$$\frac{d}{dt} \left(\frac{\delta n}{n} - \frac{\delta B}{B} \right) + \nabla_{\parallel} u_{\parallel e} = -\frac{\rho_i v_{\text{th}}}{2} \left\{ \frac{Z}{\tau} \frac{\delta n}{n}, \frac{\delta B}{B} \right\}, \quad (3.11)$$

$$\frac{\delta n}{n} = -\varphi + \overline{\hat{J}_0 h}, \quad (3.12)$$

$$\frac{u_{\parallel e}}{v_{\text{th}}} = \frac{1}{\beta_i} \hat{\nabla}_{\perp}^2 \mathcal{A} + \overline{\hat{v}_{\parallel} \hat{J}_0 h} + \mathcal{J}_{\text{ext}}, \quad (3.13)$$

$$\frac{2}{\beta_i} \frac{\delta B}{B} = \left(1 + \frac{Z}{\tau} \right) \varphi - \frac{Z}{\tau} \overline{\hat{J}_0 h} - \overline{\hat{v}_{\perp}^2 \hat{J}_1 h}. \quad (3.14)$$

Here $\tau = T_i/T_e$, $\delta n/n$ is the relative electron density perturbation (which is the same as the ion one, by quasineutrality), $u_{\parallel e}$ the parallel electron flow velocity, and overlines denote velocity integrals: $\overline{(\dots)} = (1/n_i) \int d^3 \mathbf{v} (\dots)$; note that the integrals are taken at constant \mathbf{r} and so \mathbf{R} -dependent quantities under them must be gyroaveraged at constant \mathbf{r} , hence the appearance of the \hat{J}_0 and \hat{J}_1 operators. In the above system, (3.10) is the parallel component of Ohm’s law (electron’s momentum equation), (3.11) is the electron continuity equation, (3.12) is the statement of quasineutrality, (3.13) and (3.14) are the parallel and perpendicular components, respectively, of Ampère’s law (the perpendicular one is equivalent to the statement of perpendicular pressure balance; see S09–§3.3).

In the right-hand side of (3.13), we have added a forcing term for the Alfvénic perturbations, which can be viewed as arising from a model external (nondimensionalised) “AW-antenna” current $\mathcal{J}_{\text{ext}} \equiv j_{\parallel \text{ext}}/en_e v_{\text{th}}$ (e.g., [TenBarge *et al.* 2014](#)). In the right-hand side of (3.10), we have added a resistive term (η is the magnetic diffusivity) to represent dissipation of energy into electron heat and to allow flux unfreezing at small scales (an important concern: see [Eyink 2015, 2018](#); [Boozer 2018](#)). Formally, this effect is outside the mass-ratio ordering that gave us the hybrid equations introduced above and would have to be brought in alongside electron inertia and electron-collisional effects (see S09–§7.12 and [Zocco & Schekochihin 2011](#)), but we can treat the resistive term as a representative for all of that as far as magnetic reconnection and free-energy thermalisation on electrons are concerned.⁸ This is reasonable because the precise details of how the energy is removed

does, or, indeed, is: a cascade to smaller scales, in pursuit of dissipation. In such a cascade, the smallest scales are typically reached in \sim one turnover time, regardless of how wide the full range of available scales is. Therefore, formally, any system of equations restricted to a subrange of scales is only valid for \sim one turnover time; “non-ideal” effects associated with dissipation at smaller scales come in after that (e.g., ideal-MHD solutions do not stay ideal for long, however small is the resistivity or other flux-unfreezing effects; see, e.g., [Boozer 2018](#)). This limited validity is, however, sufficient for analysing basic linear and nonlinear interactions that govern the transfer of energy through the scale subrange that is under consideration, as long as this transfer can be assumed local to this subrange. The approximate equations can also be usefully simulated numerically as long as some regularisation at small scales is provided and assuming that the nature of this regularisation is unimportant—i.e., that as long as a free-energy sink is present at the smallest scale of the considered subrange, its detailed microphysics does not affect the behaviour of larger scales (this, of course, does not always have to be the case, but tends to be).

⁸Equation (3.10) is the electron parallel momentum equation, representing the force balance between the parallel electric field (the left-hand side), parallel pressure gradient (the first term on the right-hand side) and the collisional drag force, which is the resistive term. Technically

from the system should not matter, so long as it happens at scales smaller than the ion Larmor scale and does not introduce artificial coupling between ions and electrons.⁹ These features—forcing and resistivity—will be useful in working out free-energy budgets.

3.4. Free-Energy Budget

The δf gyrokinetics conserves (except for explicit sources and sinks) a quadratic norm of the perturbations, known as the free energy (see S09–§3.4 and references therein):

$$W = \int \frac{d^3\mathbf{r}}{V} \left(\sum_s \int d^3\mathbf{v} \frac{T_s \delta f_s^2}{2F_{0s}} + \frac{|\delta\mathbf{B}|^2}{8\pi} \right), \quad (3.15)$$

where V is the volume of the plasma. Here the perturbed ion distribution function is given by (3.6), the perturbed electron distribution function under the mass-ratio expansion is $\delta f_e = (\delta n/n)F_{0e}$ (see S09–§4.4), and so, in our notation,

$$W = \frac{v_{\text{th}}^2}{4} \int \frac{d^3\mathbf{r}}{V} \left[\frac{\overline{\langle h^2 \rangle_{\mathbf{r}}}}{F_0} - \varphi^2 - 2\varphi \frac{\delta n}{n} + \frac{Z}{\tau} \frac{\delta n^2}{n^2} + \frac{2}{\beta_i} \left(|\hat{\nabla}_{\perp} \mathcal{A}|^2 + \frac{\delta B^2}{B^2} \right) \right], \quad (3.16)$$

where we have dropped the prefactor of $m_i n_i$.

Since $\int d^3\mathbf{r} \overline{\langle h^2 \rangle_{\mathbf{r}}}/F_0 = \int d^3\mathbf{R} h^2/F_0$, we may derive the evolution equation for W by multiplying (3.7) by h/F_0 , integrating over the entire GK phase space and using (3.10–3.14) opportunely. The result is

$$\frac{dW}{dt} = \varepsilon_{\text{AW}} + \varepsilon_{\text{compr}} - Q_i - Q_e, \quad (3.17)$$

where the sources are the injection rates of the Alfvénic and compressive perturbations,

$$\varepsilon_{\text{AW}} = v_{\text{th}}^2 \int \frac{d^3\mathbf{r}}{V} \frac{\partial \mathcal{A}}{\partial t} \mathcal{J}_{\text{ext}} = - \int \frac{d^3\mathbf{r}}{V} \mathbf{E} \cdot \mathbf{j}_{\text{ext}}, \quad (3.18)$$

$$\varepsilon_{\text{compr}} = \int \frac{d^3\mathbf{r}}{V} a_{\text{ext}} v_{\parallel} \overline{\hat{J}_0 h} = \int \frac{d^3\mathbf{r}}{V} a_{\text{ext}} u_{\parallel i}, \quad (3.19)$$

speaking, the latter is proportional to the difference between the electron velocity $u_{\parallel e}$ and the ion velocity $u_{\parallel i} = v_{\parallel} \hat{J}_0 h$, which is worked out from (3.13). Including normalisations, the resistive term is then $\nu_{ei}(u_{\parallel e} - u_{\parallel i})cm_e/e\rho_i B_0 = \eta(\nabla_{\perp}^2 \mathcal{A} + \beta_i \mathcal{J}_{\text{ext}}/\rho_i^2)$, where ν_{ei} is the electron-ion collision frequency and $\eta = \nu_{ei} d_e^2$. However, if η is small, it will only matter when it multiplies ∇_{\perp}^2 , as \mathcal{A} develops small-scale structure. Since we assume \mathcal{J}_{ext} to be a large-scale quantity, it can be dropped wherever it multiplies η .

⁹A minor nuance is that, in numerical practice, resistivity alone is usually insufficient to terminate a turbulent cascade described by (3.10) and (3.11)—one must have a small-scale regularisation term in (3.11) as well (Kawazura & Barnes 2018). Formally, such a term would represent collisionless and/or collisional electron damping at and below the electron Larmor scale. This too is electron heating. For the purposes of analytical energy budgets considered in this paper, the resistive term is a sufficient representative for it.

and the sinks are the ion and electron heating rates:¹⁰

$$Q_i = -\frac{v_{\text{th}}^2}{2} \int \frac{d^3\mathbf{R}}{V} \frac{hC[h]}{F_0} \geq 0, \quad (3.20)$$

$$Q_e = \eta \frac{v_{\text{th}}^2}{\beta_i \rho_i^2} \int \frac{d^3\mathbf{r}}{V} |\hat{\nabla}_{\perp}^2 \mathcal{A}|^2 = \eta \int \frac{d^3\mathbf{r}}{V} \frac{|\nabla_{\perp}^2 A_{\parallel}|^2}{4\pi m_i n_i} \geq 0. \quad (3.21)$$

We have restored dimensions these expressions to make their physical meaning more transparent. Note that in (3.18), the final expression—the work done by the electric field against the external current—is obtained by noticing that there is a perpendicular current associated with $j_{\parallel\text{ext}}$, which is small in the GK expansion (because, to avoid injecting charges, $\nabla \cdot \mathbf{j}_{\text{ext}} = 0$) and so, to lowest order in k_{\parallel}/k_{\perp} ,

$$\int \frac{d^3\mathbf{r}}{V} \frac{1}{c} \frac{\partial A_{\parallel}}{\partial t} j_{\parallel\text{ext}} = \int \frac{d^3\mathbf{r}}{V} \frac{1}{c} \frac{\partial \mathbf{A}}{\partial t} \cdot \mathbf{j}_{\text{ext}} = \int \frac{d^3\mathbf{r}}{V} \left(\frac{1}{c} \frac{\partial \mathbf{A}}{\partial t} + \nabla \phi \right) \cdot \mathbf{j}_{\text{ext}}, \quad (3.22)$$

with the expression for $-\mathbf{E}$ able to be completed with $\nabla \phi$ under the integral because $\nabla \cdot \mathbf{j}_{\text{ext}} = 0$.

In steady state, (3.17) is the overall free-energy budget, which says that the total injection is equal to the total dissipation. The main purpose of this paper is to work out more restrictive energy budgets that constrain Q_i and Q_e separately.

3.5. Separating Alfvénic Perturbations

We now rearrange the perturbed distribution function in a way that has the effect of separating the Alfvénic part of the distribution function from its “compressive” part:¹¹

$$h = \langle \varphi \rangle_{\mathbf{R}} F_0 + g = \hat{J}_0 \varphi F_0 + g \quad \Rightarrow \quad \delta f = (\langle \varphi \rangle_{\mathbf{R}} - \varphi) F_0 + g, \quad g = \langle \delta f \rangle_{\mathbf{R}}. \quad (3.23)$$

The field equations (3.12–3.14) become

$$\frac{\delta n}{n} = -(1 - \hat{\Gamma}_0) \varphi + \overline{\hat{J}_0 g}, \quad (3.24)$$

$$\frac{u_{\parallel e}}{v_{\text{th}}} = \frac{1}{\beta_i} \hat{\nabla}_{\perp}^2 \mathcal{A} + \overline{\hat{v}_{\parallel} \hat{J}_0 g} + \mathcal{J}_{\text{ext}}, \quad (3.25)$$

$$\frac{2}{\beta_i} \frac{\delta B}{B} = -\frac{Z}{\tau} \frac{\delta n}{n} + (1 - \hat{\Gamma}_1) \varphi - \overline{\hat{v}_{\perp}^2 \hat{J}_1 g}, \quad (3.26)$$

where two more Bessel operators have arisen:

$$\hat{\Gamma}_0 \leftrightarrow \overline{J_0^2(a) F_0} = I_0(\alpha) e^{-\alpha} = 1 - \alpha + \dots, \quad \alpha = \frac{k_{\perp}^2 \rho_i^2}{2} \leftrightarrow -\frac{1}{2} \hat{\nabla}_{\perp}^2, \quad (3.27)$$

$$\hat{\Gamma}_1 \leftrightarrow \overline{\hat{v}_{\perp}^2 \frac{2J_1(a)J_0(a)}{a} F_0} = -[I_0(\alpha) e^{-\alpha}]' = 1 - \frac{3}{2}\alpha + \dots \quad (3.28)$$

¹⁰If we had retained the $\eta \mathcal{J}_{\text{ext}}$ term in (3.10) (dismissed in footnote 8) and the ion–electron part of $C[h]$, the electron heating term would have turned out to be $Q_e = \nu_{ei} (Zm_e/m_i) \int d^3\mathbf{r} (u_{\parallel e} - u_{\parallel i})^2 / V = (4\pi\eta/c^2) \int d^3\mathbf{r} j_{\parallel}^2 / V$, the total Ohmic heating. This is the same as (3.21) if we drop all terms that are small in the mass-ratio expansion, only retaining instances of η multiplying the highest spatial derivatives of \mathcal{A} .

¹¹Note that this is a different rearrangement than in S09–§5.1 and so the subsequent derivation, while similar in spirit to S09–§5, is different in detail. We shall see that this is a more convenient approach.

The GK equation (3.7), rewritten in terms of g , becomes

$$\begin{aligned} \frac{\partial}{\partial t} \left(g - \hat{v}_\perp^2 \hat{J}_1 \frac{\delta B}{B} F_0 \right) + \frac{\rho_i v_{\text{th}}}{2} \left(\left\langle \langle \varphi \rangle_{\mathbf{R}}, g - \hat{v}_\perp^2 \hat{J}_1 \frac{\delta B}{B} F_0 \right\rangle + \left\langle \hat{v}_\perp^2 \hat{J}_1 \frac{\delta B}{B}, g \right\rangle \right) \\ + v_{\parallel} \left\langle \nabla_{\parallel} \left(g + \frac{Z}{\tau} \frac{\delta n}{n} F_0 \right) + \rho_i \{ \mathcal{A} - \langle \mathcal{A} \rangle_{\mathbf{R}}, \varphi - \langle \varphi \rangle_{\mathbf{R}} \} F_0 \right\rangle_{\mathbf{R}} \\ = C [g + \langle \varphi \rangle_{\mathbf{R}} F_0] + \frac{2v_{\parallel} \langle a_{\text{ext}} \rangle_{\mathbf{R}}}{v_{\text{th}}^2} F_0. \end{aligned} \quad (3.29)$$

This has been derived by using (3.10) to express $\langle \partial \mathcal{A} / \partial t \rangle_{\mathbf{R}}$ and after some manipulation of gyroaverages.¹²

In terms of g , the free energy (3.16) becomes

$$W = \frac{v_{\text{th}}^2}{4} \int \frac{d^3 \mathbf{r}}{V} \left[\frac{\langle g^2 \rangle_{\mathbf{r}}}{F_0} + \varphi (1 - \hat{\Gamma}_0) \varphi + \frac{Z}{\tau} \left| (1 - \hat{\Gamma}_0) \varphi - \hat{J}_0 g \right|^2 + \frac{2}{\beta_i} \left(|\hat{\nabla}_\perp \mathcal{A}|^2 + \frac{\delta B^2}{B^2} \right) \right], \quad (3.30)$$

where, by definition, $(1/V) \int d^3 \mathbf{r} \varphi (1 - \hat{\Gamma}_0) \varphi = \sum_{\mathbf{k}} (1 - \Gamma_0) |\varphi_{\mathbf{k}}|^2$.

For some upcoming derivations, it will be useful to have the zeroth moment of (3.29). We integrate (3.29) over velocities at constant \mathbf{r} , use (3.24) to express $\hat{J}_0 g$ and subtract (3.11) from the resulting equation, using (3.25) for $u_{\parallel e}$ and so far neglecting nothing. The outcome is

$$\begin{aligned} \frac{d}{dt} \left[(1 - \hat{\Gamma}_0) \varphi + (1 - \hat{\Gamma}_1) \frac{\delta B}{B} \right] - v_{\text{th}} \nabla_{\parallel} \left(\frac{1}{\beta_i} \hat{\nabla}_\perp^2 \mathcal{A} + \mathcal{J}_{\text{ext}} \right) = \rho_i \overline{\langle \{ \langle \mathcal{A} \rangle_{\mathbf{R}} - \mathcal{A}, v_{\parallel} g \} \rangle_{\mathbf{r}}} \\ - \frac{\rho_i v_{\text{th}}}{2} \left[\overline{\left\langle \left\langle \langle \varphi \rangle_{\mathbf{R}} - \varphi, g - \hat{v}_\perp^2 \hat{J}_1 \frac{\delta B}{B} F_0 \right\rangle + \left\langle \hat{v}_\perp^2 \hat{J}_1 \frac{\delta B}{B}, g \right\rangle \right\rangle_{\mathbf{r}}} - \left\langle \frac{Z}{\tau} \frac{\delta n}{n}, \frac{\delta B}{B} \right\rangle \right] \\ + \overline{\langle C [g + \langle \varphi \rangle_{\mathbf{R}} F_0] \rangle_{\mathbf{r}}}. \end{aligned} \quad (3.31)$$

Note that (3.10) and (3.31) have the makings of the RMHD system (3.3): this emerges from any long-wavelength approximation where one can neglect the δn term in (3.10), as well as $(1 - \hat{\Gamma}_1) \delta B / B$ and all of the right-hand side of (3.31). This is indeed how RMHD is derived from gyrokinetics in the limit of $k_\perp \rho_i \ll 1$ (S09-§§5.2, 5.3). Below, we shall apply somewhat different orderings to work out the reduced dynamics at low beta.

4. Reduced Dynamics and Heating at Low Beta

We shall now show that no ion heating occurs in the low-beta regime, viz., at $\beta_i \ll 1$. The problem has two governing parameters, β_i and $\beta_e = Z\beta_i/\tau$. There are two interesting limits:

- (i) $\beta_e \sim \beta_i \ll 1$ ($Z/\tau \sim 1$)—this section,
- (ii) $\beta_e \sim 1$ and $\beta_i \ll 1$ ($Z/\tau \sim \beta_i^{-1} \gg 1$, cold ions)—section 5.

¹²If we are to be consistent, we must retain in (3.29) a forcing term associated with the resistive term in (3.10). As we explained in footnote 8, the full form of this resistive term is $\nu_{ei}(u_{\parallel e} - u_{\parallel i})cm_e/e\rho_i B_0 = \nu_{ie}(u_{\parallel e} - u_{\parallel i})/v_{\text{th}}$, where $\nu_{ie} = (m_e n_e / m_i n_i) \nu_{ei}$ is the ion-electron collision frequency. The additional term that belongs in the left-hand side of (3.29) is, therefore, $2\nu_{ie} v_{\parallel} \langle u_{\parallel e} - u_{\parallel i} \rangle_{\mathbf{R}} F_0 / v_{\text{th}}^2$, which is minus the ion-electron friction force. But this is cancelled by the linearised ion-electron collision operator, which, to lowest order in the mass-ratio expansion, is just the ion-electron friction (see, e.g., Helander & Sigmar 2005). Thus, from now on, we may drop the resistive term in (3.29) as long as the collision operator in this equation is understood to contain the ion-ion collisions only.

In considering these limits, we shall make use of the notation and equations introduced in section 3. Namely, our starting point is the system consisting of the six equations (3.10–3.11), (3.24–3.26) and (3.29) for six fields \mathcal{A} , φ , δn , δB , $u_{\parallel e}$ and g .

4.1. Ordering

Working in the limit $\beta_e \sim \beta_i \ll 1$, we let

$$\frac{Z}{\tau} = \frac{\beta_e}{\beta_i} \sim 1, \quad k_{\perp} \rho_i \sim 1, \quad (4.1)$$

the latter assumption meaning that we are able to treat the Larmor-scale transition directly.

Since we wish to be able to handle Alfvénic perturbations, and since we wish their linear frequency ($k_{\parallel} v_A$) and their nonlinear interaction rate ($k_{\perp} u_{\perp}$) to be able to be comparable, we stipulate

$$\frac{\delta B_{\perp}}{B} \sim \frac{u_{\perp}}{v_A} \sim \frac{k_{\parallel}}{k_{\perp}} \sim \epsilon, \quad (4.2)$$

where ϵ is the basic GK expansion parameter, with no further β_i -related factors, of which we shall now keep a close watch. In view of (4.1), this assumption implies

$$\frac{\delta B_{\perp}}{B} \sim \frac{k_{\perp} A_{\parallel}}{B_0} \sim k_{\perp} \rho_i \mathcal{A} \quad \Rightarrow \quad \mathcal{A} \sim \epsilon, \quad (4.3)$$

$$\frac{u_{\perp}}{v_A} \sim \frac{ck_{\perp} \phi}{v_A B_0} \sim k_{\perp} \rho_i \sqrt{\beta_i} \varphi \quad \Rightarrow \quad \varphi \sim \frac{\epsilon}{\sqrt{\beta_i}}. \quad (4.4)$$

Examination of (3.24–3.26) then suggests that

$$\frac{\delta n}{n} \sim \frac{g}{F_0} \sim \varphi \sim \frac{\epsilon}{\sqrt{\beta_i}}, \quad \frac{\delta B}{B} \sim \epsilon \sqrt{\beta_i}. \quad (4.5)$$

4.2. Equations

With this ordering, the kinetic equation (3.29) becomes, to lowest order in β_i ,

$$\frac{\partial g}{\partial t} + \frac{\rho_i v_{\text{th}}}{2} \{ \langle \varphi \rangle_{\mathbf{R}}, g \} = C[g + \langle \varphi \rangle_{\mathbf{R}} F_0] + \frac{2v_{\parallel} \langle a_{\text{ext}} \rangle_{\mathbf{R}}}{v_{\text{th}}^2} F_0. \quad (4.6)$$

If we ignore collisions and assume no external forcing ($a_{\text{ext}} = 0$), then $g = 0$ is a good solution of this equation (these assumptions will be relaxed in section 4.5). The field equations (3.24–3.26) turn into simple constitutive relations

$$\frac{\delta n}{n} = -(1 - \hat{I}_0) \varphi, \quad \frac{u_{\parallel e}}{v_{\text{th}}} = \frac{1}{\beta_i} \hat{\nabla}_{\perp}^2 \mathcal{A} + \mathcal{J}_{\text{ext}}, \quad \frac{\delta B}{B} = \frac{\beta_i}{2} \left[\frac{Z}{\tau} (1 - \hat{I}_0) + (1 - \hat{I}_1) \right] \varphi. \quad (4.7)$$

Using the first two of these in (3.10–3.11), we find that the latter become, to lowest order,

$$\frac{\partial \mathcal{A}}{\partial t} + \frac{v_{\text{th}}}{2} \nabla_{\parallel} \left[1 + \frac{Z}{\tau} (1 - \hat{I}_0) \right] \varphi = \eta \nabla_{\perp}^2 \mathcal{A}, \quad (4.8)$$

$$\frac{d}{dt} (1 - \hat{I}_0) \varphi = \frac{v_{\text{th}}}{\beta_i} \nabla_{\parallel} \hat{\nabla}_{\perp}^2 \mathcal{A} + v_{\text{th}} \nabla_{\parallel} \mathcal{J}_{\text{ext}}. \quad (4.9)$$

These equations are the same as those derived by Zocco & Schekochihin (2011) in the limit of ultra-low beta ($\beta_e \sim m_e/m_i$), except the electron inertia and the coupling to non-isothermal electron kinetics have now been lost—the price (painless to pay, in the context of present study, because energetics are not affected) for considering somewhat higher β_e .

The system of equations (4.8–4.9) turns into RMHD (3.3) when $k_{\perp}\rho_i \ll 1$: this is shown by using $1 - \hat{\Gamma}_0 \approx -\hat{\nabla}_{\perp}^2/2$ [see (3.27)]. In the opposite limit $k_{\perp}\rho_i \gg 1$, using $1 - \hat{\Gamma}_0 \approx 1$, one obtains the $\beta \ll 1$ limit of the ‘‘Electron RMHD’’ equations (ERMHD; see S09–§7.2 or Boldyrev *et al.* 2013). In the more conventional notation involving stream and flux functions [defined in (3.1)], they are

$$\frac{\partial\Psi}{\partial t} = v_A \left(1 + \frac{Z}{\tau}\right) \nabla_{\parallel}\Phi + \eta\nabla_{\perp}^2\Psi, \quad \frac{\partial\Phi}{\partial t} = -\frac{v_A}{2}\nabla_{\parallel}\rho_i^2\nabla_{\perp}^2\Psi \quad (4.10)$$

(we have dropped \mathcal{J}_{ext} because it occurs at large scales). The relationship between the magnetic field and Ψ is still the same as in (3.2). While Φ is still the stream function for the $\mathbf{E} \times \mathbf{B}$ velocity, this is now the velocity of the electron flow (ions are much slower because of gyroaveraging). These equations describe what is sometimes referred to as the turbulence of Kinetic Alfvén Waves (KAW)—although, like the Alfvénic (RMHD) turbulence in the inertial range, it is expected to be strong and critically balanced and so does not literally consist of waves (see S09–§7.5 and Cho & Lazarian 2004, 2009; Boldyrev & Perez 2012; TenBarge & Howes 2012; TenBarge *et al.* 2013; Boldyrev & Loureiro 2019).

If we consider cold ions, $Z/\tau \gg 1$ (but not so cold as to break $\beta_e \ll 1$), there is an intermediate regime with

$$\frac{Z}{\tau}(1 - \Gamma_0) \approx k_{\perp}^2\rho_s^2 \sim 1, \quad \rho_s = \sqrt{\frac{Z}{2\tau}}\rho_i = \frac{c_s}{\Omega}, \quad c_s = \sqrt{\frac{ZT_e}{m_i}}, \quad (4.11)$$

where c_s is the sound speed and $\rho_s \gg \rho_i$ is the ‘‘sound radius’’, setting a transition scale. In this regime, the electron-pressure-gradient term [the right-hand side of (3.11)] is non-negligible and so the AW dynamics become dispersive: using (3.1) and (4.11) in (4.8–4.9), we arrive at a simple modification of RMHD equations (3.3) (cf. Bian & Tsiklauri 2009):

$$\frac{\partial\Psi}{\partial t} = v_A\nabla_{\parallel}(1 - \rho_s^2\nabla_{\perp}^2)\Phi, \quad \frac{d}{dt}\nabla_{\perp}^2\Phi = v_A\nabla_{\parallel}\nabla_{\perp}^2\Psi. \quad (4.12)$$

There is then a second transition in (4.8–4.9) at $k_{\perp}\rho_i \sim 1$, to ERMHD (4.10).

4.3. Linear Theory

These transitions become particularly transparent if we consider the linear dispersion relation for the system (4.8–4.9):

$$\omega^2 = k_{\parallel}^2 v_A^2 \frac{k_{\perp}^2 \rho_i^2}{2} \left(\frac{1}{1 - \Gamma_0} + \frac{Z}{\tau} \right) \approx \begin{cases} k_{\parallel}^2 v_A^2 (1 + k_{\perp}^2 \rho_s^2), & k_{\perp} \rho_i \ll 1, \\ \frac{1 + Z/\tau}{2} k_{\parallel}^2 v_A^2 k_{\perp}^2 \rho_i^2, & k_{\perp} \rho_i \gg 1. \end{cases} \quad (4.13)$$

The $k_{\perp}\rho_i \ll 1$ limit is the Alfvén wave with the dispersive correction due to the electron-pressure gradient. The $k_{\perp}\rho_i \gg 1$ limit is the KAW dispersion relation with $\beta \ll 1$ (see S09–§7.3). When $Z/\tau \gg 1$, it becomes $\omega^2 \approx k_{\parallel}^2 v_A^2 k_{\perp}^2 \rho_s^2$ and so the transition between the long- and short-wavelength frequencies is seamless. Thus, in this limit, the transition between the AW and KAW cascades occurs at $k_{\perp}\rho_s \sim 1$.

4.4. Free-Energy Budget

The nonlinear system (4.8–4.9) has a conserved energy

$$W = \frac{v_{\text{th}}^2}{4} \int \frac{d^3\mathbf{r}}{V} \left[\varphi(1 - \hat{\Gamma}_0)\varphi + \frac{Z}{\tau} |(1 - \hat{\Gamma}_0)\varphi|^2 + \frac{2}{\beta_i} |\hat{\nabla}_{\perp}\mathcal{A}|^2 \right], \quad (4.14)$$

which is the appropriate low-beta, $g = 0$ limit of (3.30). Note that, whereas $\delta n/n$ does appear in (4.14) (the second term), δB is energetically (and dynamically) insignificant [see (4.7)].

At $k_{\perp}\rho_s \ll 1$, (4.14) reduces to the energy of Alfvén waves

$$W_{\text{AW}} = \frac{1}{2} \int \frac{d^3\mathbf{r}}{V} (|\nabla_{\perp}\Phi|^2 + |\nabla_{\perp}\Psi|^2) = \frac{1}{2} \int \frac{d^3\mathbf{r}}{V} (|\mathbf{u}_{\perp}|^2 + |\mathbf{b}_{\perp}|^2), \quad (4.15)$$

conserved by RMHD (3.3). When $k_{\perp}\rho_s \sim 1$ but $k_{\perp}\rho_i \ll 1$,

$$W = \frac{1}{2} \int \frac{d^3\mathbf{r}}{V} (|\nabla_{\perp}\Phi|^2 + \rho_s^2 |\nabla_{\perp}^2\Phi|^2 + |\nabla_{\perp}\Psi|^2), \quad (4.16)$$

the energy of the system (4.12). At $k_{\perp}\rho_i \gg 1$, W becomes the energy of low-beta KAW perturbations described by (4.10):¹³

$$W_{\text{KAW}} = \int \frac{d^3\mathbf{r}}{V} \left[\left(1 + \frac{Z}{\tau}\right) \frac{\Phi^2}{\rho_i^2} + \frac{1}{2} |\nabla_{\perp}\Psi|^2 \right]. \quad (4.17)$$

The existence of the invariant (4.14), valid uniformly at small, order-unity and large $k_{\perp}\rho_i$, means that no damping of anything and, therefore, no ion heating occurs at any wave number, until resistivity kicks in and causes electron heating; it is easy to ascertain that

$$\frac{dW}{dt} = \varepsilon_{\text{AW}} - Q_e, \quad (4.18)$$

where ε_{AW} is given by (3.18) and Q_e by (3.21). In steady state, $Q_e = \varepsilon_{\text{AW}}$.

4.5. Energy Partition in the Presence of Compressive Cascade

In the above, we assumed the $g = 0$ solution for the kinetic equation (4.6). This corresponds to a situation in which only Alfvénic perturbations are stirred up at the largest scales: indeed, the relations (4.7) imply that the compressive fields δn and δB peter out at $k_{\perp}\rho_i \ll 1$. Let us now relax this assumption. Mathematically, this would correspond, e.g., to restoring the external parallel acceleration term in (4.6). The variance of the forced kinetic scalar described by (4.6) with $a_{\text{ext}} \neq 0$ is conserved by the nonlinearity:

$$\frac{d}{dt} \frac{v_{\text{th}}^2}{4} \int \frac{d^3\mathbf{r}}{V} \overline{\frac{g^2}{F_0}} - \frac{v_{\text{th}}^2}{2} \int \frac{d^3\mathbf{r}}{V} \overline{\left\langle \frac{gC[g + \langle\varphi\rangle_{\mathbf{R}}F_0]}{F_0} \right\rangle_{\mathbf{r}}} = \int \frac{d^3\mathbf{r}}{V} \overline{a_{\text{ext}} \langle v_{\parallel} g \rangle_{\mathbf{r}}} = \varepsilon_{\text{compr}}, \quad (4.19)$$

where $\varepsilon_{\text{compr}}$ is the energy flux in the compressive cascade [cf. (3.19)]. In steady state ($d/dt = 0$), we have a balance between this compressive input power and the collisional terms [cf. (3.17)]:

$$\varepsilon_{\text{compr}} = Q_i + Q_x, \quad Q_x = \frac{v_{\text{th}}^2}{2} \int \frac{d^3\mathbf{r}}{V} \overline{\langle\langle\varphi\rangle_{\mathbf{R}}C[h]\rangle_{\mathbf{r}}} = \frac{v_{\text{th}}^2}{2} \int \frac{d^3\mathbf{r}}{V} \overline{\varphi \langle C[h] \rangle_{\mathbf{r}}}, \quad (4.20)$$

where Q_i is given by (3.20). Thus, all the compressive energy becomes ion heat, with the exception of the collisional energy exchange Q_x with Alfvénic perturbations, which is, as we are about to argue, small when collisions are weak. The implication is that all the Alfvénic energy is destined, via the AW cascade smoothly transitioning into the KAW cascade, to be dissipated into electron heat,

$$\varepsilon_{\text{AW}} = \varepsilon_{\text{KAW}} = Q_e. \quad (4.21)$$

¹³Note the typo in S09-§7.8, where this is derived: a missing factor of 2 in front of Φ^2 in Eq. (246).

We will confirm this directly in section 4.6.

If the collision frequency is small compared to the forcing or nonlinear-advection time scales in (4.6), the only way for the collision terms to balance the finite energy flux is for g to develop small scales in phase space, thus activating large derivatives in $C[h]$. This is indeed what happens, as the nonlinear term successfully pushes g towards small scales in both \mathbf{R} and v_\perp , viz., towards $\delta v_\perp/v_{\text{th}} \sim (k_\perp \rho_i)^{-1} \ll 1$, via a process known as the entropy cascade (see S09–§7.9). This is a route to ion heating that requires no parallel streaming and is, therefore, the only feasible one for the effectively 2D kinetic equation (4.6), where the parallel streaming has been ordered out due to low β_i (cf. Tatsuno et al. 2009; Plunk et al. 2010). Recent numerical results by Kawazura et al. (2019) appear to confirm the presence of such an ion-heating route in low-beta GK turbulence.

The ion heating rate Q_i [see (3.20)] is positive definite and by this process it will be rendered finite, i.e., independent of the ion collision rate, however small the latter is. Let us estimate the size of Q_x in comparison to Q_i . Clearly, only the parts of φ and h that vary on fine scales in position and velocity space matter in Q_x and Q_i , the contribution from large scales being small because the collision frequency is small. The GK collision operator is a diffusion operator both in velocity and position (see, e.g., Abel et al. 2008), with the size of the position and velocity gradients comparable in the entropy cascade. At $k_\perp \rho_i \gg 1$, when collisions become important,

$$Q_i \sim v_{\text{th}}^2 \nu_{ii} (k_\perp \rho_i)^2 \frac{h^2}{F_0^2}, \quad (4.22)$$

$$Q_x \sim v_{\text{th}}^2 \nu_{ii} (k_\perp \rho_i)^{3/2} \frac{h}{F_0} \varphi \sim v_{\text{th}}^2 \nu_{ii} k_\perp \rho_i \frac{h^2}{F_0^2}, \quad (4.23)$$

where ν_{ii} is the ion collision frequency. Thus, $Q_x \ll Q_i$. Here Q_x loses out compared to Q_i by one factor of $(k_\perp \rho_i)^{1/2}$ because of the gyroaveraging under the velocity integral of $C[h]$ and by another factor of $(k_\perp \rho_i)^{1/2}$ because, as will be evident from (4.24–4.25), we must order $\varphi \sim \widehat{J}_0 g \sim (k_\perp \rho_i)^{-1/2} h/F_0$ in order for the compressive perturbations to have any relevance. In fact, (4.23) is probably an overestimate because Q_x is not sign-definite and so there will also be a tendency for the small-scale variation within it to average out under integration. In any event, it is clear that when collisions are weak, the collisional energy exchange can be neglected.

4.6. Effect of Compressive Cascade on Alfvénic Cascade

For completeness, let us ascertain that the notion that non-zero g has no energetic effect on the AW and KAW cascades is consistent with the dynamical equations for the latter. We allow $g/F_0 \sim \varphi$ as per (4.5). In this case, $v_\parallel \widehat{J}_0 g$ is still one-order subdominant in (3.25) and $\delta B/B$ is still small compared to $\delta n/n$, but there is now a contribution from g to $\delta n/n$ in (3.24). The resulting pair of equations, replacing (4.8–4.9), is

$$\frac{\partial \mathcal{A}}{\partial t} + \frac{v_{\text{th}}}{2} \nabla_\parallel \left\{ \varphi + \frac{Z}{\tau} \left[(1 - \widehat{I}_0) \varphi - \overline{\widehat{J}_0 g} \right] \right\} = \eta \nabla_\perp^2 \mathcal{A}, \quad (4.24)$$

$$\frac{d}{dt} \left[(1 - \widehat{I}_0) \varphi - \overline{\widehat{J}_0 g} \right] - \frac{v_{\text{th}}}{\beta_i} \nabla_\parallel \widehat{\nabla}_\perp^2 \mathcal{A} = v_{\text{th}} \nabla_\parallel \mathcal{J}_{\text{ext}}, \quad (4.25)$$

coupled to (4.6).

The quantity in the square brackets in (4.24) and (4.25) is $-\delta n/n$, so these equations can be thought of as evolution equations of \mathcal{A} and $\delta n/n$, the latter's relationship to φ

now involving g . Alternatively, (4.25) can be recast as

$$\frac{d}{dt}(1 - \hat{I}_0)\varphi - \frac{v_{\text{th}}}{\beta_i} \nabla_{\parallel} \hat{\nabla}_{\perp}^2 \mathcal{A} = v_{\text{th}} \nabla_{\parallel} \mathcal{J}_{\text{ext}} - \frac{\rho_i v_{\text{th}}}{2} \overline{\langle \langle \varphi \rangle_{\mathbf{R}} - \varphi, g \rangle_{\mathbf{r}}} + \overline{\langle C[g + \langle \varphi \rangle_{\mathbf{R}} F_0] \rangle_{\mathbf{r}}} \quad (4.26)$$

if one uses the evolution equation for $\widehat{J}_0 g$ derived by integrating (4.6) over the velocity space [(4.26) can also be obtained by applying the ordering (4.5) to (3.31)].¹⁴ This emphasises the nonlinear FLR coupling of φ to g .

These equations support a generalised version of the (collisionless) invariant (4.14):

$$\widetilde{W} = \frac{v_{\text{th}}^2}{4} \int \frac{d^3 \mathbf{r}}{V} \left[\varphi(1 - \hat{I}_0)\varphi + \frac{Z}{\tau} \left| (1 - \hat{I}_0)\varphi - \widehat{J}_0 g \right|^2 + \frac{2}{\beta_i} |\hat{\nabla}_{\perp} \mathcal{A}|^2 \right], \quad (4.27)$$

which is the low-beta limit of (3.30), excluding the variance of g , which is still conserved independently [see (4.19)]. Indeed, using (4.26) to work out the time derivative of the first term and (4.24) and (4.25) for the other two terms, we get

$$\frac{d\widetilde{W}}{dt} = \varepsilon_{\text{AW}} - Q_e + Q_x, \quad (4.28)$$

where ε_{AW} is given by (3.18), Q_e by (3.21) and Q_x in (4.20). The nonlinear terms have vanished by cancellation and because

$$\int \frac{d^3 \mathbf{r}}{V} \overline{\varphi \langle \langle \varphi \rangle_{\mathbf{R}} - \varphi, g \rangle_{\mathbf{r}}} = \int \frac{d^3 \mathbf{R}}{V} \overline{\langle \varphi \rangle_{\mathbf{R}} \langle \langle \varphi \rangle_{\mathbf{R}}, g \rangle} = 0 \quad (4.29)$$

(after swapping the order of the \mathbf{v} and \mathbf{r} integration and changing the integration variable from \mathbf{r} to \mathbf{R}).

Combining (4.28) and (4.19), we recover the overall conservation law (3.17), as indeed we must, because the free energy is

$$W = \widetilde{W} + \frac{v_{\text{th}}^2}{4} \int \frac{d^3 \mathbf{r}}{V} \frac{\langle g^2 \rangle_{\mathbf{r}}}{F_0}. \quad (4.30)$$

However, we now have more restrictive and, therefore, more informative energy balances (4.20) and (4.28) (with $d\widetilde{W}/dt = 0$ in steady state). Since, as we argued in section 4.5, Q_x is small, we conclude that

$$Q_i = \varepsilon_{\text{compr}}, \quad Q_e = \varepsilon_{\text{AW}}, \quad (4.31)$$

so compressive energy goes into ions, Alfvénic into electrons. Thus, while non-zero g does insinuate itself into the dynamics of Alfvénic perturbations, there is no energy exchange between the two cascades.

4.7. Ultra-Low Beta

Formally, there is an interesting very-low-beta limit that is outside the validity of our theory so far. Namely, if $\beta_e \sim m_e/m_i$, we can no longer use the isothermal-electron-fluid approximation introduced in section 3.3. The equations in this case are quite similar to (4.6) and (4.24–4.25), except in (4.24) there is now an electron-inertia term and a piece of parallel pressure gradient that contains a non-zero parallel electron temperature perturbation. The latter has to be calculated from the electron drift-kinetic equation, thus opening up an electron heating route via parallel heat transport and Landau damping.

¹⁴Our choice of forcing in (4.6) has ensured that the contribution of g to density is not affected and so the compressive driving does not stir up Alfvénic perturbations.

With $g = 0$, the appropriate equations were worked out by Zocco & Schekochihin (2011) and proved to be a useful model for numerical experimentation (Loureiro *et al.* 2013, 2016; Grošelj *et al.* 2017); they can be generalised to $g \neq 0$ in exactly the same way as the system (4.8–4.9) was generalised in sections 4.5 and 4.6. There is no change in the energy partition: by the same arguments as above, the energy of compressive perturbations goes into ions, the energy of Alfvénic ones into electrons.

5. Reduced Dynamics and Heating in the Hall Limit

Let us now consider the case of $\beta_e \sim 1$ and $\beta_i \ll 1$. This is the so-called Hall limit and the derivation in sections 5.1–5.4 is a reworking (in a slightly different order) of the “Hall RMHD” (S09–§E), which we will need for what follows and which turns out to have some interesting consequences for the energy partition, detailed in sections 5.5 and 5.7.

5.1. Ordering

In this limit, since $\beta_e = Z\beta_i/\tau$, the ions are cold and, as we anticipate based on section 4, the AW physics will become dispersive at $k_\perp \rho_s \sim 1$:

$$\frac{Z}{\tau} \sim \frac{1}{\beta_i} \gg 1, \quad k_\perp \rho_s \sim 1 \quad \Rightarrow \quad k_\perp \rho_i \sim \sqrt{\frac{\tau}{Z}} \sim \sqrt{\beta_i} \ll 1 \quad \Rightarrow \quad k_\perp d_i \sim 1, \quad (5.1)$$

where $d_i = \rho_i/\sqrt{\beta_i} = \rho_s\sqrt{2/\beta_e}$ is the ion inertial scale, which is of the same order as ρ_s in this limit.

We must adjust all expansions and equations accordingly. Instead of (4.3) and (4.4), we have

$$\mathcal{A} \sim \frac{\epsilon}{k_\perp \rho_i} \sim \frac{\epsilon}{\sqrt{\beta_i}}, \quad \varphi \sim \frac{\epsilon}{k_\perp \rho_i \sqrt{\beta_i}} \sim \frac{\epsilon}{\beta_i}. \quad (5.2)$$

Since the sound speed and the Alfvén speed are of the same order in this limit, viz.,

$$c_s = \sqrt{\frac{Z T_e}{m_i}} = v_{\text{th}} \sqrt{\frac{Z}{2\tau}} = v_A \sqrt{\frac{\beta_e}{2}} \sim v_A, \quad (5.3)$$

the AW and the compressive modes (slow waves) have similar frequencies. This allows us to handle both cascades simultaneously. To avoid prejudice, we order the compressive perturbations to have similar amplitudes to the Alfvénic ones:

$$\frac{\delta n}{n} \sim \frac{u_{\parallel i}}{v_A} \sim \frac{\delta B}{B} \sim \frac{\delta B_\perp}{B} \sim \epsilon, \quad (5.4)$$

where $u_{\parallel i} = \overline{v_{\parallel} \hat{J}_0 g}$ is the parallel ion flow velocity. The requirement that (3.24–3.26) be consistent with (5.4) implies that we ought to order

$$\frac{g}{F_0} \sim \frac{\epsilon}{\sqrt{\beta_i}}, \quad \overline{\hat{J}_0 g} \sim \epsilon, \quad (5.5)$$

i.e., to lowest order, the distribution function should have no density moment.

5.2. Equations

With these orderings, (3.24–3.26) become, to lowest order in β_i (and τ),

$$\bar{g} = \frac{\delta n}{n} - \frac{1}{2} \hat{\nabla}_\perp^2 \varphi, \quad u_{\parallel e} = u_{\parallel i} + v_{\text{th}} \left(\frac{1}{\beta_i} \hat{\nabla}_\perp^2 \mathcal{A} + \mathcal{J}_{\text{ext}} \right), \quad \frac{\delta n}{n} = -\frac{2}{\beta_e} \frac{\delta B}{B}. \quad (5.6)$$

The last of these equations is the balance between the magnetic and electron pressure, ions being too cold to matter. Using this relationship in (3.10–3.11), we get¹⁵

$$\frac{\partial \mathcal{A}}{\partial t} + \frac{v_{\text{th}}}{2} \nabla_{\parallel} \left(\varphi + \frac{2}{\beta_i} \frac{\delta B}{B} \right) = \eta \nabla_{\perp}^2 \mathcal{A}, \quad (5.7)$$

$$\left(1 + \frac{2}{\beta_e} \right) \frac{d}{dt} \frac{\delta B}{B} = \nabla_{\parallel} \left[u_{\parallel i} + v_{\text{th}} \left(\frac{1}{\beta_i} \hat{\nabla}_{\perp}^2 \mathcal{A} + \mathcal{J}_{\text{ext}} \right) \right]. \quad (5.8)$$

So all four fields \mathcal{A} , φ , δB and $u_{\parallel i}$ (the latter representing g) are coupled and we need two more equations to close the system.

One of these is (3.31), where applying the ordering of section 5.1 leads to the disappearance of the entire right-hand side, as well as of the δB term under the time derivative. To lowest order, therefore, we are left with a rather familiar equation [cf. the second RMHD equation in (3.3)]:

$$\frac{d}{dt} \frac{1}{2} \hat{\nabla}_{\perp}^2 \varphi + \frac{v_{\text{th}}}{\beta_i} \nabla_{\parallel} \hat{\nabla}_{\perp}^2 \mathcal{A} = -v_{\text{th}} \nabla_{\parallel} \mathcal{J}_{\text{ext}}. \quad (5.9)$$

The last required equation is the lowest-order version of the kinetic equation (3.29):

$$\frac{dg}{dt} = v_{\parallel} \nabla_{\parallel} \frac{2}{\beta_i} \frac{\delta B}{B} F_0 + C[g] + \frac{2v_{\parallel} a_{\text{ext}}}{v_{\text{th}}^2} F_0, \quad (5.10)$$

where we again used the last equation in (5.6). This is consistent with $\bar{g} = 0$ to lowest order, as anticipated in (5.5). If we split off the velocity moment from g , viz.,

$$g = \frac{2u_{\parallel i} v_{\parallel}}{v_{\text{th}}^2} F_0 + \mathcal{G}, \quad \bar{g} = 0, \quad \overline{v_{\parallel} \mathcal{G}} = 0, \quad (5.11)$$

then (5.10) becomes

$$\frac{du_{\parallel i}}{dt} = v_A^2 \nabla_{\parallel} \frac{\delta B}{B} + a_{\text{ext}}, \quad (5.12)$$

$$\frac{d\mathcal{G}}{dt} = C[\mathcal{G}]. \quad (5.13)$$

The first of these is the final equation that we needed to close the system comprising already (5.7), (5.8) and (5.9). The second equation, (5.13), describes a passively advected kinetic field, which, however, is not coupled to anything and so can be safely put to zero¹⁶—it is the kinetic version of the MHD entropy mode, whereas the rest of our equations describe linearly and nonlinearly coupled AW and slow waves (SW). Note finally that (5.9) is needed because it is not possible to calculate φ from the first and last of the field equations (5.6) and the kinetic equation (5.10). This is because, as assumed in (5.5), the density moment \bar{g} comes from the next-order part of g not captured in (5.10).

It is instructive to rewrite the Hall RMHD equations (5.7–5.9) and (5.12) in “fluid”

¹⁵The resistive term in (5.7) can, in fact, be legitimately retained only if resistivity becomes important before the Larmor scale is reached. This is possible formally, but unlikely in reality.

¹⁶Unless it is explicitly forced. The forcing that we have chosen for compressive perturbations has ended up only driving parallel ion flows. To model energy injection into \mathcal{G} , we would need to inject, e.g., temperature perturbations—physically this can happen if there is an equilibrium temperature gradient (see, e.g., Schekochihin *et al.* 2016 or Xu & Kunz 2016), but we shall not consider such equilibria here.

notation, dropping the forcing terms and resistivity (cf. Gómez *et al.* 2008):

$$\frac{\partial \Psi}{\partial t} = v_A \nabla_{\parallel} (\Phi + v_A \rho_H \mathcal{B}), \quad (5.14)$$

$$\frac{d\mathcal{B}}{dt} = \nabla_{\parallel} (v_s \mathcal{U} - \rho_H \nabla_{\perp}^2 \Psi), \quad (5.15)$$

$$\frac{d}{dt} \nabla_{\perp}^2 \Phi = v_A \nabla_{\parallel} \nabla_{\perp}^2 \Psi, \quad (5.16)$$

$$\frac{d\mathcal{U}}{dt} = v_s \nabla_{\parallel} \mathcal{B}, \quad (5.17)$$

where Φ and Ψ are defined by (3.1), we have denoted

$$\mathcal{B} = \frac{\delta B}{B} \sqrt{1 + \frac{2}{\beta_e}}, \quad \mathcal{U} = \frac{u_{\parallel i}}{v_A}, \quad (5.18)$$

and introduced the Hall transition scale

$$\rho_H = \frac{d_i}{\sqrt{1 + 2/\beta_e}} = \frac{\rho_s}{\sqrt{1 + \beta_e/2}} = \rho_i \sqrt{\frac{Z/\tau}{2 + \beta_e}} \quad (5.19)$$

and the SW phase speed

$$v_s = \frac{v_A}{\sqrt{1 + 2/\beta_e}} = \frac{c_s}{\sqrt{1 + \beta_e/2}}. \quad (5.20)$$

At $k_{\perp} \rho_H \ll 1$, the Alfvénic and the SW-like perturbations decouple from each other and revert to standard RMHD equations (see S09–§2.4): the AW equations (5.14) and (5.16) become (3.3) and the SW equations (5.15) and (5.17) become

$$\frac{d\mathcal{B}}{dt} = v_s \nabla_{\parallel} \mathcal{U}, \quad \frac{d\mathcal{U}}{dt} = v_s \nabla_{\parallel} \mathcal{B} \quad (5.21)$$

(passively advected by the AW via d/dt and ∇_{\parallel} , without energy exchange). Thus, our new system of equations (5.14–5.17) captures the RMHD regime and describes its transformation, at the Hall transition scale ρ_H , into one in which all four fields Φ , Ψ , \mathcal{B} and \mathcal{U} are coupled.

The system (5.14–5.17) also contains the low- β_e limit (4.12). This corresponds to taking the limit $v_s \rightarrow 0$. Combining (5.15) and (5.16), we get

$$\frac{d}{dt} \left(\mathcal{B} + \frac{\rho_H}{v_A} \nabla_{\perp}^2 \Phi \right) = v_s \nabla_{\parallel} \mathcal{U} \rightarrow 0 \quad \Rightarrow \quad \mathcal{B} = -\frac{\rho_H}{v_A} \nabla_{\perp}^2 \Phi. \quad (5.22)$$

Using this in (5.14) and setting $\rho_H = \rho_s$, we get the first equation in (4.12). The second is the same as (5.16). The parallel velocity in this limit decouples and cascades independently:

$$\frac{d\mathcal{U}}{dt} = 0, \quad (5.23)$$

just like \mathcal{G} does in (5.13) and like g did in (4.6).

5.3. Free Energy and Heating

The conserved free energy for (5.14–5.17) [equivalently, for (5.7–5.9) and (5.12)] is

$$\begin{aligned}\widetilde{W} &= \frac{1}{2} \int \frac{d^3\mathbf{r}}{V} \left[|\nabla_{\perp}\Phi|^2 + |\nabla_{\perp}\Psi|^2 + v_A^2 (\mathcal{U}^2 + \mathcal{B}^2) \right] \\ &= \int \frac{d^3\mathbf{r}}{V} \left[\frac{v_{\text{th}}^2}{4} \left(\frac{1}{2} |\hat{\nabla}_{\perp}\varphi|^2 + \frac{2}{\beta_i} |\hat{\nabla}_{\perp}\mathcal{A}|^2 \right) + \frac{u_{\parallel i}^2}{2} + \frac{\delta B^2}{8\pi m_i n_i} \left(1 + \frac{2}{\beta_e} \right) \right].\end{aligned}\quad (5.24)$$

The free energy has no access to \mathcal{G} , whose variance is individually conserved, as is obvious from (5.13). If we forced \mathcal{G} (without breaking the ordering of section 5.1), the free energy injected in this way would remain decoupled and travel all through the Hall range of scales unconcerned with the wave dynamics, eventually arriving at $k_{\perp}\rho_i \sim 1$ and transiting into the sub-Larmor-scale ion entropy cascade and eventually into ion heat (see section 5.7.4). As we already mentioned in footnote 16, a natural physical way in which \mathcal{G} might be forced is by the presence of an ion temperature gradient. However, there cannot be net heating of the plasma by turbulence produced by temperature gradients: any energy thus “borrowed” from the ion thermal bath may only be redistributed between species (Abel *et al.* 2013). In the present case, all of it is destined for ions.

The first two terms in (5.24) are the Alfvénic energy (4.15), conserved by the RMHD (3.3); the last two terms are the slow-wave energy

$$W_{\text{SW}} = \frac{v_A^2}{2} \int \frac{d^3\mathbf{r}}{V} (\mathcal{U}^2 + \mathcal{B}^2), \quad (5.25)$$

conserved by (5.21). When $\beta_e \ll 1$, the substitution of (5.22) turns (5.24) into (4.16), with the \mathcal{U}^2 part of the free energy splitting off, destined for ion heating. In contrast, at $\beta_e \sim 1$, the decoupling between the Alfvénic and compressive cascades is broken at $k_{\perp}\rho_H \sim 1$, so we can no longer conclude that the former must heat electrons and the latter ions. In order to work out what happens (see section 5.5.4 for a preview of the answer), we must shift our focus to $k_{\perp}\rho_i \sim 1$ (section 5.7), but for that, we must first investigate into what kind of turbulence the Hall turbulence turns at $k_{\perp}\rho_H \gg 1$ (section 5.5). In working this out, we will find linear theory to be a valuable guide.

5.4. Linear Theory

The dispersion relation is

$$(\omega^2 - \omega_{\text{AW}}^2)(\omega^2 - \omega_{\text{SW}}^2) = \omega^2 \omega_{\text{KAW}}^2, \quad (5.26)$$

where $\omega_{\text{AW}} = k_{\parallel}v_A$ is the AW frequency, $\omega_{\text{SW}} = k_{\parallel}v_s$ the SW frequency and $\omega_{\text{KAW}} = k_{\parallel}v_A k_{\perp}\rho_H$ the KAW frequency in the $Z/\tau \gg 1$ limit (cf. S09–§7.3). There is no damping of anything here because ions cannot stream along the field lines as fast as waves propagate [see (5.10)].

At $k_{\perp}\rho_H \ll 1$, $\omega_{\text{KAW}} \ll \omega_{\text{AW}}, \omega_{\text{SW}}$ and we recover from (5.26) four low-frequency MHD waves

$$\omega = \pm\omega_{\text{AW}}, \quad \omega = \pm\omega_{\text{SW}}. \quad (5.27)$$

At $k_{\perp}\rho_H \gg 1$, if $\omega \gg \omega_{\text{AW}}, \omega_{\text{SW}}$, the linear response assumes its KAW form:¹⁷

$$\omega = \pm\omega_{\text{KAW}} = \pm k_{\parallel}v_A k_{\perp}\rho_H. \quad (5.28)$$

¹⁷As it did in the $\beta_e \ll 1$ limit treated in section 4.3. It is also not hard to see that, at $\beta_e \ll 1$, $\omega_{\text{SW}} \ll \omega_{\text{AW}}$ and the Alfvénic branch in (5.26) obeys the $k_{\perp}\rho_i \ll 1$ version of (4.13).

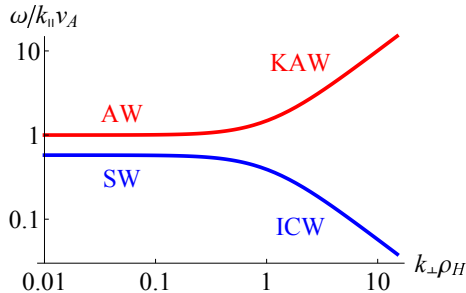


FIGURE 1. Solutions (5.33) of the Hall dispersion relation (5.26) with $\beta_e = 1$.

This is not particularly surprising: the KAW response is the Alfvénic response with (nearly) immobile ions—and the ion-flow terms in the two magnetic-field equations (5.14) and (5.15) do indeed become subdominant at $k_\perp \rho_H \gg 1$. Linearly, the KAW are then described by

$$\frac{\partial \Psi}{\partial t} = v_A^2 \rho_H \frac{\partial \mathcal{B}}{\partial z}, \quad \frac{\partial \mathcal{B}}{\partial t} = -\rho_H \frac{\partial}{\partial z} \nabla_\perp^2 \Psi. \quad (5.29)$$

In the Hall limit, there is nothing particularly kinetic about kinetic Alfvén waves, so they should probably be called Hall Alfvén waves (but are sometimes called whistlers); we shall keep the KAW moniker to avoid multiplying entities beyond necessity.

There is more to the story at $k_\perp \rho_H \gg 1$. In this limit, besides the two KAW, (5.26) has two other, low-frequency, solutions:

$$\omega = \pm \frac{\omega_{\text{AW}} \omega_{\text{SW}}}{\omega_{\text{KAW}}} = \pm \frac{k_\parallel v_s}{k_\perp \rho_H} = \pm \Omega \frac{k_\parallel}{k_\perp} \equiv \pm \omega_{\text{ICW}}. \quad (5.30)$$

These are oblique ion cyclotron waves (ICW; cf. [Sahraoui et al. 2007](#)). For these perturbations, (5.14) and (5.15) become quasistatic, viz.,

$$\mathcal{B} = -\frac{\Phi}{v_A \rho_H}, \quad \nabla_\perp^2 \Psi = \frac{v_s}{\rho_H} \mathcal{U} = \Omega \mathcal{U}, \quad (5.31)$$

and, consequently, the linearised versions of (5.16) and (5.17) turn into

$$\frac{\partial}{\partial t} \nabla_\perp^2 \Phi = \Omega \frac{\partial u_{\parallel i}}{\partial z}, \quad \frac{\partial u_{\parallel i}}{\partial t} = -\Omega \frac{\partial \Phi}{\partial z}. \quad (5.32)$$

It is more transparent here to go back from \mathcal{U} [defined in (5.18)] to $u_{\parallel i}$ as the Alfvénic normalisation is no longer physically relevant. These equations, and the corresponding dispersion relation (5.30), are mathematically the same as the equations and the dispersion relation for inertial waves in rigidly rotating (with angular velocity $\Omega/2$) neutral fluids (see, e.g., [Nazarenko & Schekochihin 2011](#); [Davidson 2013](#)). We shall see momentarily that the analogy survives also nonlinearly and that, therefore, ICW turbulence displays some familiar features.

Finally, figure 1 shows the full solutions of (5.26),

$$\omega^2 = \frac{k_\parallel^2 v_A^2}{2} \left\{ 1 + \sigma^2 + k_\perp^2 \rho_H^2 \pm \sqrt{[k_\perp^2 \rho_H^2 + (1 + \sigma)^2][k_\perp^2 \rho_H^2 + (1 - \sigma)^2]} \right\}, \quad (5.33)$$

where

$$\sigma = \frac{v_s}{v_A} = \frac{1}{\sqrt{1 + 2/\beta_e}} \quad (5.34)$$

(the only parameter in the problem). Note that there is no mode conversion, the AW

continuously turn into KAW and SW into ICW. The two curves separate ever further at smaller β_e , tending towards the limit described by (4.12) and (5.22).

5.5. Hall Turbulence at Short Wavelengths

The nature of Hall turbulence at $k_\perp \rho_H \gg 1$ is determined by the way in which fast (KAW) and slow (ICW) perturbations interact with themselves and (potentially) with each other.

We are dealing with a two-time-scale problem, so let us split all our fields into slow and fast components, with “slow” defined as the average of the relevant field over the KAW period and “fast” as the difference between that and the exact field:

$$\Psi = \overline{\Psi} + \tilde{\Psi}, \quad \Phi = \overline{\Phi} + \tilde{\Phi}, \quad \mathcal{B} = \overline{\mathcal{B}} + \tilde{\mathcal{B}}, \quad \mathcal{U} = \overline{\mathcal{U}} + \tilde{\mathcal{U}}. \quad (5.35)$$

In everything that follows, overbar will mean KAW-time-scale averaging and overtilde will designate KAW-time-scale quantities, which average to zero (with apologies to the reader, who should now forget what overbars and overtildes have been used for previously). The slow quantities will represent the ICW turbulence and the fast ones the KAW turbulence.

We shall venture an *a priori* guess that the two cascades will decouple completely at $k_\perp \rho_H \gg 1$, work out the scalings of all the fields on that basis and then confirm *a posteriori* that those are consistent with such a decoupling. Namely, we anticipate that the nonlinear version of the KAW equations (5.29) will be

$$\frac{\partial \tilde{\Psi}}{\partial t} = v_A^2 \rho_H \widetilde{\nabla_\parallel \tilde{\mathcal{B}}}, \quad \frac{\partial \tilde{\mathcal{B}}}{\partial t} = -\rho_H \widetilde{\nabla_\parallel \nabla_\perp^2 \tilde{\Psi}}, \quad \nabla_\parallel = \frac{\partial}{\partial z} + \frac{1}{v_A} \{\tilde{\Psi}, \dots\}, \quad (5.36)$$

and the nonlinear version of the ICW equations (5.32)

$$\frac{d}{dt} \nabla_\perp^2 \overline{\Phi} = \Omega v_A \frac{\partial \overline{\mathcal{U}}}{\partial z}, \quad \frac{d \overline{\mathcal{U}}}{dt} = -\frac{\Omega}{v_A} \frac{\partial \overline{\Phi}}{\partial z}, \quad \frac{d}{dt} = \frac{\partial}{\partial t} + \{\overline{\Phi}, \dots\}. \quad (5.37)$$

In each case, the other two fields play a subordinate role: for KAW turbulence, from (5.16) and (5.17),

$$\frac{\partial}{\partial t} \nabla_\perp^2 \tilde{\Phi} = v_A \widetilde{\nabla_\parallel \nabla_\perp^2 \tilde{\Psi}}, \quad \frac{\partial \tilde{\mathcal{U}}}{\partial t} = v_s \widetilde{\nabla_\parallel \tilde{\mathcal{B}}}; \quad (5.38)$$

for ICW turbulence, (5.31) hold nonlinearly, viz.,

$$\overline{\mathcal{B}} = -\frac{\overline{\Phi}}{v_A \rho_H}, \quad \nabla_\perp^2 \overline{\Psi} = \Omega \overline{\mathcal{U}}. \quad (5.39)$$

The physics of these “constitutive relations” will be made transparent in (5.86). Note that the first equation in (5.38) combined with the second equation in (5.36) also turns into a “constitutive relation” between $\tilde{\mathcal{B}}$ and $\tilde{\Phi}$ [cf. (5.22)]:

$$\nabla_\perp^2 \tilde{\Phi} = -\frac{v_A}{\rho_H} \tilde{\mathcal{B}}. \quad (5.40)$$

The pieces of the free energy (5.24) individually conserved by the systems (5.36) and (5.37) are, respectively,

$$W_{\text{KAW}} = \frac{1}{2} \int \frac{d^3 \mathbf{r}}{V} \left[|\nabla_\perp \tilde{\Psi}|^2 + v_A^2 \tilde{\mathcal{B}}^2 \right], \quad (5.41)$$

$$W_{\text{ICW}} = \frac{1}{2} \int \frac{d^3 \mathbf{r}}{V} \left[|\nabla_\perp \overline{\Phi}|^2 + v_A^2 \overline{\mathcal{U}}^2 \right]. \quad (5.42)$$

Here W_{ICW} is just the kinetic energy of the ion motion, perpendicular plus parallel, whereas W_{KAW} is the total magnetic energy plus the free energy of the electron distribution—the latter is the $\delta n^2/n^2$ term in (3.16), now absorbed into $\tilde{\mathcal{B}}^2$ by way of the last equation in (5.6).

We are now going to work out all the relevant scalings for KAW (section 5.5.1) and ICW (section 5.5.2) turbulence, then use these scalings to confirm that (5.36–5.39) are correct (section 5.5.3), and finally propose what the energy partition in these circumstances should be (section 5.5.4).

5.5.1. KAW Scalings

The scalings for a critically balanced cascade of KAW-like fluctuations are a standard proposition (see S09-§7.5 and Cho & Lazarian 2004).¹⁸ The magnetic energy has a constant flux ε_{KAW} , with the cascade time scale set by the magnetic nonlinearity inside ∇_{\parallel} in, e.g., the first equation in (5.36):

$$(k_{\perp} \tilde{\Psi})^2 \tau_{\text{nl}}^{-1} \sim \varepsilon_{\text{KAW}}, \quad \tau_{\text{nl}}^{-1} \sim v_{\text{A}} \rho_{\text{H}} k_{\perp}^2 \tilde{\mathcal{B}}. \quad (5.43)$$

The relationship between $\tilde{\mathcal{B}}$ and $\tilde{\Psi}$, and hence the scaling of field amplitudes, is then fixed by the second equation in (5.36):

$$\tilde{\mathcal{B}} \sim \omega_{\text{KAW}}^{-1} \rho_{\text{H}} k_{\parallel \text{KAW}} k_{\perp}^2 \tilde{\Psi} \sim \frac{k_{\perp} \tilde{\Psi}}{v_{\text{A}}} \sim \left(\frac{\varepsilon_{\text{KAW}}}{\rho_{\text{H}} v_{\text{A}}^3} \right)^{1/3} k_{\perp}^{-2/3}, \quad (5.44)$$

the last relation following from (5.43). Finally, the relationship between the wave frequency ω_{KAW} (and, therefore, $k_{\parallel \text{KAW}}$) and the nonlinear decorrelation rate τ_{nl}^{-1} (and, therefore, k_{\perp}) is set by the critical-balance conjecture:

$$\omega_{\text{KAW}} = k_{\parallel \text{KAW}} v_{\text{A}} k_{\perp} \rho_{\text{H}} \sim \tau_{\text{nl}}^{-1} \quad \Rightarrow \quad k_{\parallel \text{KAW}} \sim \left(\frac{\varepsilon_{\text{KAW}}}{\rho_{\text{H}} v_{\text{A}}^3} \right)^{1/3} k_{\perp}^{1/3}. \quad (5.45)$$

The two subordinate fields are found from (5.38):

$$\tilde{\Phi} \sim \omega_{\text{KAW}}^{-1} k_{\parallel \text{KAW}} v_{\text{A}} \tilde{\Psi} = \frac{\tilde{\Psi}}{k_{\perp} \rho_{\text{H}}}, \quad \tilde{U} \sim \omega_{\text{KAW}}^{-1} k_{\parallel \text{KAW}} v_{\text{s}} \tilde{\mathcal{B}} = \frac{v_{\text{s}}}{v_{\text{A}}} \frac{\tilde{\mathcal{B}}}{k_{\perp} \rho_{\text{H}}}. \quad (5.46)$$

It follows from all this that the magnetic and velocity spectra are

$$E_{\tilde{\mathcal{B}}} \propto k_{\perp}^{-7/3}, \quad E_{\tilde{u}} \propto k_{\perp}^{-13/3} \quad (5.47)$$

(cf. Galtier & Buchlin 2007; Meyrand & Galtier 2012).

5.5.2. ICW Scalings

The scalings for a critically balanced ICW cascade are perhaps less well established, but also known, in the guise of the scalings for rotating hydrodynamic turbulence (Nazarenko & Schekochihin 2011). Assuming constant energy flux ε_{ICW} and using the first equation in (5.37), we find the Kolmogorov scaling (which is no surprise, the

¹⁸Various theoretical considerations (Boldyrev & Perez 2012; Boldyrev *et al.* 2013; Meyrand & Galtier 2013; Loureiro & Boldyrev 2017; Boldyrev & Loureiro 2019), prompted by observational evidence (Alexandrova *et al.* 2009; Sahnouli *et al.* 2010; Chen 2016), suggest that these “naïve” scalings may need some subtle corrections. We shall opt for simplicity over modernity and ignore those subtleties. We need these scalings as a vehicle for estimating the size of KAW and ICW perturbations relative to each other and we do not believe that a more sophisticated theory of the KAW cascade will change our conclusions in any essential way.

nonlinear coupling being hydrodynamic):

$$(k_{\perp}\bar{\Phi})^2\tau_{\text{nl}}^{-1} \sim \varepsilon_{\text{ICW}}, \quad \tau_{\text{nl}}^{-1} \sim k_{\perp}^2\bar{\Phi} \quad \Rightarrow \quad k_{\perp}\bar{\Phi} \sim \varepsilon_{\text{ICW}}^{1/3}k_{\perp}^{-1/3}. \quad (5.48)$$

From either equation in (5.37),

$$\bar{U} \sim \frac{k_{\perp}\bar{\Phi}}{v_{\text{A}}}. \quad (5.49)$$

The critical-balance conjecture implies

$$\omega_{\text{ICW}} = \Omega \frac{k_{\parallel\text{ICW}}}{k_{\perp}} \sim \tau_{\text{nl}}^{-1} \quad \Rightarrow \quad k_{\parallel\text{ICW}} \sim \frac{\varepsilon_{\text{ICW}}^{1/3}}{\Omega} k_{\perp}^{5/3}. \quad (5.50)$$

Interestingly, it follows from (5.50) that ICW turbulence becomes *less* anisotropic at smaller scales.¹⁹ Finally, the subordinate fields (5.39) are

$$\bar{B} \sim \frac{\bar{\Phi}}{v_{\text{A}}\rho_{\text{H}}} \sim \frac{\bar{U}}{k_{\perp}\rho_{\text{H}}}, \quad \frac{k_{\perp}\bar{\Psi}}{v_{\text{A}}} \sim \frac{v_{\text{s}}}{v_{\text{A}}} \frac{\bar{U}}{k_{\perp}\rho_{\text{H}}}. \quad (5.51)$$

The velocity and magnetic energy spectra are, therefore,

$$E_{\bar{u}} \propto k_{\perp}^{-5/3}, \quad E_{\bar{B}} \propto k_{\perp}^{-11/3} \quad (5.52)$$

(cf. Krishan & Mahajan 2004; Galtier & Buchlin 2007; Meyrand & Galtier 2012).

5.5.3. Decoupling of Cascades

The above scalings appear to be consistent with the numerical evidence recently reported by Meyrand *et al.* (2018), who solved the traditional Hall-MHD equations that effectively describe the $\beta_e \gg 1$ limit of our system ($v_{\text{s}} = v_{\text{A}}$ and $\rho_{\text{H}} = d_i$). They did see $E_{\bar{u}} \ll E_{\bar{B}} \ll E_{\bar{\Psi}} \ll E_{\bar{\pi}} \propto k_{\perp}^{-5/3}$; the $k_{\perp}^{-7/3}$ and $k_{\perp}^{-11/3}$ spectra of the magnetic perturbations associated with the two different wave modes [see (5.47) and (5.52)] had previously been extracted numerically from Hall MHD by Meyrand & Galtier (2012) (and from a shell model by Galtier & Buchlin 2007). Unlike us, Meyrand *et al.* (2018) think that the KAW turbulence is weak, rather than critically balanced, but we consider the evidence that they present in fact consistent with the possibility of a critically balanced KAW cascade: in particular, both their KAW fluctuations and their ICW fluctuations have broad frequency spectra and are spatially anisotropic in a scale-dependent way, the former becoming more anisotropic and the latter less, as k_{\perp} increases—in agreement with (5.45) and (5.50). They also see striking evidence that $k_{\parallel\text{KAW}} \ll k_{\parallel\text{ICW}}$, which is indeed what (5.45) and (5.50) imply. Finally, and crucially, they show quite unambiguously that energy exchange between velocity and magnetic fields (and, therefore, between ICW and KAW fluctuations) peters out at $k_{\perp}d_i \gg 1$, i.e., the two cascades are energetically decoupled.

As promised above, we now confirm that the scalings of sections 5.5.1 and 5.5.2, if adopted as orderings, do indeed allow the two cascades to decouple (an impatient reader willing to trust us may skip to section 5.5.4). Let

$$\epsilon = \frac{(\varepsilon_{\text{ICW}}\rho_{\text{H}})^{1/3}}{v_{\text{A}}} \sim \frac{(\varepsilon_{\text{KAW}}\rho_{\text{H}})^{1/3}}{v_{\text{A}}}, \quad \delta = \frac{1}{(k_{\perp}\rho_{\text{H}})^{1/3}}. \quad (5.53)$$

Here ϵ is just the GK expansion parameter that must enter all field amplitudes. The only

¹⁹Isotropy is achieved at $k_{\perp} \sim \Omega^{3/2}\varepsilon_{\text{ICW}}^{-1/2}$, known as the Zeman (1994) scale in the context of inertial waves. This scale is, however, outside the GK ordering and so is formally smaller than any scale present in our considerations.

nontrivial choice about ϵ is that $\epsilon_{\text{KAW}} \sim \epsilon_{\text{ICW}}$, i.e., that the KAW and ICW fluctuations receive *a priori* comparable amounts of energy—equivalently, we assume that the KAW and ICW amplitudes are similar at the Hall transition scale (at $k_{\perp}\rho_{\text{H}} \sim 1$). We now use δ as a subsidiary ordering parameter for the Hall-MHD equations (5.14–5.17):

$$\frac{k_{\perp}\bar{\Phi}}{v_{\text{A}}} \sim \bar{\mathcal{U}} \sim \epsilon\delta, \quad \frac{k_{\perp}\bar{\Psi}}{v_{\text{A}}} \sim \epsilon\sigma\delta^4, \quad \bar{\mathcal{B}} \sim \epsilon\delta^4, \quad (5.54)$$

$$k_{\parallel\text{ICW}}\rho_{\text{H}} \sim \epsilon\sigma^{-1}\delta^{-5}, \quad \frac{\omega_{\text{ICW}}}{\Omega} \sim \epsilon\sigma^{-1}\delta^{-2}, \quad (5.55)$$

$$\frac{k_{\perp}\tilde{\Psi}}{v_{\text{A}}} \sim \tilde{\mathcal{B}} \sim \epsilon\delta^2, \quad \frac{k_{\perp}\tilde{\Phi}}{v_{\text{A}}} \sim \epsilon\delta^5, \quad \tilde{\mathcal{U}} \sim \epsilon\sigma\delta^5, \quad (5.56)$$

$$k_{\parallel\text{KAW}}\rho_{\text{H}} \sim \epsilon\delta^{-1}, \quad \frac{\omega_{\text{KAW}}}{\Omega} \sim \epsilon\sigma^{-1}\delta^{-4}, \quad (5.57)$$

where σ is defined in (5.34).

Applying the decomposition (5.35) and the above ordering to (5.14), we get, keeping two lowest orders,

$$\frac{\partial\tilde{\Psi}}{\partial t} = v_{\text{A}}\frac{\partial}{\partial z}(\bar{\Phi} + v_{\text{A}}\rho_{\text{H}}\bar{\mathcal{B}}) + v_{\text{A}}^2\rho_{\text{H}}\nabla_{\parallel}\tilde{\mathcal{B}}, \quad \nabla_{\parallel} = \frac{\partial}{\partial z} + \frac{1}{v_{\text{A}}}\{\tilde{\Psi}, \dots\}. \quad (5.58)$$

Averaging this equation over the KAW time scale gives us

$$v_{\text{A}}\frac{\partial}{\partial z}(\bar{\Phi} + v_{\text{A}}\rho_{\text{H}}\bar{\mathcal{B}}) + v_{\text{A}}\rho_{\text{H}}\overline{\{\tilde{\Psi}, \tilde{\mathcal{B}}\}} = 0. \quad (5.59)$$

Subtracting this from (5.58), we end up with the first KAW equation in (5.36). Retaining the lowest order only in (5.59) results in the first ICW constitutive relation in (5.39), assuming that we can ignore any additive corrections to this that are constant along the magnetic field.

From (5.17), again keeping only two lowest orders, we get

$$\frac{d\bar{\mathcal{U}}}{dt} + \frac{\partial\tilde{\mathcal{U}}}{\partial t} = v_{\text{s}}\left(\frac{\partial\bar{\mathcal{B}}}{\partial z} + \nabla_{\parallel}\tilde{\mathcal{B}}\right), \quad \frac{d}{dt} = \frac{\partial}{\partial t} + \{\bar{\Phi}, \dots\}. \quad (5.60)$$

Averaging and using (5.59) gives us

$$\frac{d\bar{\mathcal{U}}}{dt} = v_{\text{s}}\left(\frac{\partial\bar{\mathcal{B}}}{\partial z} + \frac{1}{v_{\text{A}}}\overline{\{\tilde{\Psi}, \tilde{\mathcal{B}}\}}\right) = -\frac{v_{\text{s}}}{v_{\text{A}}\rho_{\text{H}}}\frac{\partial\bar{\Phi}}{\partial z}, \quad (5.61)$$

which is the second ICW equation in (5.37). Subtracting (5.61) from (5.60) leaves us with the second equation in (5.38), describing small parallel ion flows associated with KAW.

Continuing in the same vein, we find that (5.15) becomes, to two lowest orders,

$$\frac{\partial\tilde{\mathcal{B}}}{\partial t} = \frac{\partial}{\partial z}(v_{\text{s}}\bar{\mathcal{U}} - \rho_{\text{H}}\nabla_{\perp}^2\bar{\Psi}) - \rho_{\text{H}}\nabla_{\parallel}\nabla_{\perp}^2\tilde{\Psi}. \quad (5.62)$$

The average of this is

$$\frac{\partial}{\partial z}(v_{\text{s}}\bar{\mathcal{U}} - \rho_{\text{H}}\nabla_{\perp}^2\bar{\Psi}) - \frac{\rho_{\text{H}}}{v_{\text{A}}}\overline{\{\tilde{\Psi}, \nabla_{\perp}^2\tilde{\Psi}\}} = 0, \quad (5.63)$$

which, to lowest order, becomes the second ICW constitutive relation in (5.39) (again ignoring any contributions that do not vary along the magnetic field). Subtracting (5.63) from (5.62) gets us the second KAW equation in (5.36).

Finally, (5.16) to two lowest orders is

$$\frac{d}{dt} \nabla_{\perp}^2 \bar{\Phi} + \frac{\partial}{\partial t} \nabla_{\perp}^2 \tilde{\Phi} = v_A \left(\frac{\partial}{\partial z} \nabla_{\perp}^2 \bar{\Psi} + \nabla_{\parallel} \nabla_{\perp}^2 \tilde{\Psi} \right). \quad (5.64)$$

Its average is, via (5.63),

$$\frac{d}{dt} \nabla_{\perp}^2 \bar{\Phi} = v_A \frac{\partial}{\partial z} \nabla_{\perp}^2 \bar{\Psi} + \overline{\{\tilde{\Psi}, \nabla_{\perp}^2 \tilde{\Psi}\}} = \frac{v_s v_A}{\rho_H} \frac{\partial \bar{\mathcal{U}}}{\partial z}, \quad (5.65)$$

which is the first ICW equation in (5.37). Subtracting (5.65) from (5.64), we get the first equation in (5.38) for the small perpendicular flows present in KAW.

Thus, the equations for decoupled KAW and ICW cascades, (5.36–5.39), which were our basis for developing the scalings in sections 5.5.1 and 5.5.2, can indeed be extracted from Hall equations (5.14–5.17) if those scalings are assumed.²⁰ Consistency is the least—and the most—that we can ask for in this approach.

5.5.4. Energy Partition

We anticipate, and will prove in section 5.7, that the sub-Hall-scale KAW cascade all goes into the sub-Larmor-scale KAW cascade and thence to electron heating, whereas the ICW cascade is destined for ion-entropy cascade and thence to ion heating. Thus, *in the Hall regime, the energy partition is decided at the Hall scale* ρ_H . While we do not know how to determine this energy partition rigorously, a plausible conjecture can be made.

The only parameter in the problem is the ratio $\sigma = v_s/v_A$ [equivalently, β_e : see (5.34)]. As explained at the end of section 5.2, (5.14–5.17) reduce to (4.12) in the limit of $\sigma \ll 1$ (low β_e). This happens because, sufficiently far into that limit, the finite- $k_{\perp} \rho_H$ contribution to \mathcal{B} from the Alfvénic fluctuations overwhelms the SW part of \mathcal{B} [see (5.22)], while what remains of the SW cascades independently according to (5.23), unbothered by the Hall-scale transition. The result is again (4.31): the Alfvénic energy goes into electrons, the compressive one into ions.

In contrast, when $\sigma \sim 1$, there are no small parameters left in the problem and all time scales and all parts of the free energy (5.24) are of the same order at $k_{\perp} \rho_H \sim 1$. At $k_{\perp} \rho_H \ll 1$, Φ and Ψ fluctuations carry ε_{AW} , while \mathcal{U} and \mathcal{B} fluctuations carry $\varepsilon_{\text{compr}}$. On the other side of the transition, at $k_{\perp} \rho_H \gg 1$, the Ψ and \mathcal{B} fluctuations (the magnetic energy) are picked up by the KAW cascade (ε_{KAW}) and the Φ and \mathcal{U} fluctuations (the kinetic energy) by the ICW cascade (ε_{ICW}). It is then natural to conjecture an equal split of the power of the original MHD cascade between ε_{KAW} and ε_{ICW} , and, therefore, between electron and ion heating—independently of the relative size of ε_{AW} and $\varepsilon_{\text{compr}}$:

$$Q_e \sim \varepsilon_{\text{KAW}} \sim \frac{\varepsilon_{\text{AW}} + \varepsilon_{\text{compr}}}{2} \sim \varepsilon_{\text{ICW}} \sim Q_i. \quad (5.66)$$

Numerical simulations of the full system (5.14–5.17) with external driving are needed (and will be done) to test this reasoning. A parameter scan in σ should reveal a gradual transition from $[Q_i/Q_e]_{\sigma \rightarrow 0} \rightarrow \varepsilon_{\text{compr}}/\varepsilon_{\text{AW}}$ to $[Q_i/Q_e]_{\sigma \rightarrow 1} \rightarrow 1$.

²⁰Turbulence-theory *literati* might appreciate an amusing mathematical similarity between the situation that has emerged here and the rigidly rotating MHD turbulence at *large* scales, which also features two co-existing cascades—of inertial and magnetostrophic waves—with dispersion relations and, therefore, scalings similar to ICW and KAW, respectively (Galtier 2014; Bell & Nazarenko 2019).

5.6. *Helicities*

Before, as promised, moving on to the Larmor-scale dynamics, let us, for the sake of completeness and for the benefit of those readers who might be interested in Hall RMHD turbulence *per se*, offer some discussion of other invariants of the system (5.14–5.17). Famously, Hall MHD equations conserve two helicities, magnetic and “hybrid” (Turner 1986; Mahajan & Yoshida 1998). However, in Hall RMHD, owing to the presence of a strong background magnetic field, magnetic helicity is not conserved, except in 2D:

$$H = \int \frac{d^3\mathbf{r}}{V} \Psi \mathcal{B}, \quad \frac{dH}{dt} = \int \frac{d^3\mathbf{r}}{V} \left(v_s \Psi \frac{\partial \mathcal{U}}{\partial z} + v_A \mathcal{B} \frac{\partial \Phi}{\partial z} \right) \quad (5.67)$$

(see S09–§F.4 and references therein for a discussion of helicity non-conservation in a system with a mean field). What is conserved, however, is the sum of three other “helicities” present in the system, viz., the Alfvénic cross-helicity, the compressive cross-helicity and the kinetic helicity (note that $\nabla_{\perp}^2 \Phi$ is the z component of the vorticity of the plasma motions):

$$X = \int \frac{d^3\mathbf{r}}{V} \left[(\nabla_{\perp} \Phi) \cdot (\nabla_{\perp} \Psi) + \frac{v_A^3}{v_s} \mathcal{U} \left(\mathcal{B} + \frac{\rho_H}{v_A} \nabla_{\perp}^2 \Phi \right) \right]. \quad (5.68)$$

Note that the Hall MHD “hybrid” helicity referred to above is then just $H - (\rho_H/v_A)X$ (not conserved because H is not conserved).

In the RMHD limit ($k_{\perp} \rho_H \ll 1$), X loses its last term (the kinetic helicity) and turns into the standard RMHD cross-helicity, whose conservation reflects the energetic decoupling of the cascades of the four Elsasser fields $\Phi \pm \Psi$ and $\mathcal{U} \pm \mathcal{B}$ (see S09–§2.7). In the opposite limit, $k_{\perp} \rho_H \gg 1$, when Hall RMHD splits into the KAW equations (5.36) and the ICW equations (5.37), each of these systems conserves its own piece of X :

$$X_{\text{KAW}} = \int \frac{d^3\mathbf{r}}{V} \tilde{\Psi} \tilde{\mathcal{B}}, \quad X_{\text{ICW}} = \frac{v_A^2}{\Omega} \int \frac{d^3\mathbf{r}}{V} \bar{\mathcal{U}} \nabla_{\perp}^2 \bar{\Phi}. \quad (5.69)$$

The first of these is the helicity of the KAW turbulence, which is in fact the cross-helicity (5.68) by way of (5.40) and integration by parts (cf. S09–§F.3); the second is the kinetic helicity of the ICW turbulence—the last term in (5.68), dominant when $k_{\perp} \rho_H \gg 1$.

While X_{KAW} or X_{ICW} being non-zero would indicate an imbalance between counterpropagating KAW-like or ICW-like perturbations, respectively, there is no corollary that such counterpropagating perturbations have energetically decoupled cascades in the way that Elsasser fields do in RMHD. This is because while the conserved quantity X is the difference between the “energies” of the generalised Elsasser fields $\Phi \pm \Psi$ and $\mathcal{U} \pm (\mathcal{B} + \rho_H \nabla_{\perp}^2 \Phi / v_A)$, the sum of these “energies” is not the free energy (5.24) and is not conserved, and neither, therefore, are these “energies” conserved individually. Note also that these fields are not the eigenfunctions associated with the counterpropagating modes: in the $k_{\perp} \rho_H \gg 1$ limit, those are $v_A \tilde{\mathcal{B}} \mp k_{\perp} \tilde{\Psi}$ for $\omega = \pm \omega_{\text{KAW}}$ and $v_A \bar{\mathcal{U}} \pm k_{\perp} \bar{\Phi}$ for $\omega = \pm \omega_{\text{ICW}}$. The energies of these fields are not individually conserved either.

The presence of extra invariants does open the possibility of dual or even triple cascades in Hall RMHD turbulence: in particular, X_{KAW} will cascade to larger scales if it is injected at small scales (see S09–§F.6; Cho & Kim 2016 and references therein), whereas X_{ICW} is expected to cascade forward, together with the free energy (Chen *et al.* 2003; Banerjee & Galtier 2016). Thus, the Hall RMHD system can offer some considerable rewards to a devoted turbulence theorist.

5.7. Larmor-Scale Transition

We are now going to prove that, once the KAW and ICW cascades hit the Larmor scale, the former will be channelled into electron heating (via a sub-Larmor KAW cascade) and the latter into ion heating (via an electrostatic ion entropy cascade). What follows is formally necessary, as due diligence, but a reader who is not a particular GK aficionada need not read it if she trusts our algebra.²¹ Qualitative physics discussion resumes in section 6.

5.7.1. Ordering

We continue to assume the Hall ordering of the temperature ratio vs. plasma beta [see (5.1)], but focus on scales that are of the order of the Larmor radius, a regime that does not appear to have been studied before:

$$\frac{Z}{\tau} \sim \frac{1}{\beta_i} \gg 1, \quad k_{\perp} \rho_i \sim 1 \quad \Rightarrow \quad k_{\perp} \rho_H \sim k_{\perp} \rho_i \sqrt{\frac{Z}{\tau}} \sim \frac{1}{\sqrt{\beta_i}} \gg 1. \quad (5.70)$$

The ordering of the time scales and amplitudes must now be adjusted. How to do this can be deduced *a priori* from the $k_{\perp} \rho_H \gg 1$ orderings (5.53–5.57) by taking them to the illegitimate extreme $k_{\perp} \rho_H \sim 1/\sqrt{\beta_i}$, or $\delta \sim \beta_i^{1/6}$. Having obtained the orderings, we will then backtrack to the hybrid ion-electron equations of sections 3.3 and 3.5 and derive a new set of equations valid under our new ordering.

Reverting to our old notation, we convert the δ orderings (5.54–5.57) into β_i orderings using $\delta \sim \beta_i^{1/6}$, $\sigma \sim 1$, $k_{\parallel} \rho_H \sim k_{\parallel} \rho_i \sqrt{\beta_i}$, and

$$\frac{k_{\perp} \Phi}{v_A} \sim \frac{k_{\perp} \rho_i v_{\text{th}}}{v_A} \varphi \sim \varphi \sqrt{\beta_i}, \quad \mathcal{U} \sim \frac{u_{\parallel i}}{v_{\text{th}}} \sqrt{\beta_i}, \quad \frac{k_{\perp} \Psi}{v_A} \sim k_{\perp} \rho_i \mathcal{A} \sim \mathcal{A}, \quad \mathcal{B} \sim \frac{\delta B}{B} \quad (5.71)$$

[recall (3.1) and (5.18)]. The resulting ordering is

$$\bar{\varphi} \sim \frac{\bar{u}_{\parallel i}}{v_{\text{th}}} \sim \frac{\bar{g}}{F_0} \sim \epsilon \beta_i^{-1/3}, \quad \bar{\mathcal{A}} \sim \frac{\delta \bar{B}}{B} \sim \frac{\delta \bar{n}}{n} \sim \epsilon \beta_i^{2/3}, \quad \frac{\omega_{\text{ICW}}}{\Omega} \sim \frac{k_{\parallel \text{ICW}} v_{\text{th}}}{\Omega} \sim \epsilon \beta_i^{-1/3}, \quad (5.72)$$

$$\tilde{\varphi} \sim \frac{\tilde{u}_{\parallel i}}{v_{\text{th}}} \sim \frac{\tilde{g}}{F_0} \sim \tilde{\mathcal{A}} \sim \frac{\delta \tilde{n}}{n} \sim \epsilon \beta_i^{1/3}, \quad \frac{\omega_{\text{KAW}}}{\Omega} \sim \epsilon \beta_i^{-2/3}, \quad \frac{k_{\parallel \text{KAW}} v_{\text{th}}}{\Omega} \sim \epsilon \beta_i^{1/3}, \quad (5.73)$$

where bars and tildes continue to mean averaged and fluctuating quantities over the KAW time scale. Note that for ICW, the wave frequency and the ion streaming rate have turned out to be the same size, whereas for KAW, the former is much larger than the latter. This is the basic physical reason why ICW will couple into ion kinetics and, eventually, ion heating, while KAW will not.

5.7.2. Field Equations

The field equations (3.24–3.26) are linear, so can be split cleanly into slow- and fast-varying parts. To lowest order (in all cases, $\sim \beta_i^{-1/3}$ for the slow fields and $\sim \beta_i^{-2/3}$ for

²¹This said, (5.86) and (5.89) are perhaps of some technical interest, showing the electrostatic nature of the ICW cascade.

the fast ones), they are²²

$$(1 - \hat{I}_0)\tilde{\varphi} = -\frac{\delta\tilde{n}}{n} + \frac{1}{n_i} \int d^3\mathbf{v} \hat{J}_0 \tilde{g}, \quad (5.74)$$

$$\frac{\tilde{u}_{\parallel e}}{v_{\text{th}}} = \frac{1}{\beta_i} \hat{\nabla}_{\perp}^2 \tilde{\mathcal{A}} + \tilde{\mathcal{J}}_{\text{ext}}, \quad (5.75)$$

$$\frac{Z}{\tau} \frac{\delta\tilde{n}}{n} = -\frac{2}{\beta_i} \frac{\delta\tilde{B}}{B}, \quad (5.76)$$

$$(1 - \hat{I}_0)\bar{\varphi} = \frac{1}{n_i} \int d^3\mathbf{v} \hat{J}_0 \bar{g}, \quad (5.77)$$

$$\frac{\bar{u}_{\parallel e}}{v_{\text{th}}} = \frac{1}{\beta_i} \hat{\nabla}_{\perp}^2 \bar{\mathcal{A}} + \frac{\bar{u}_{\parallel i}}{v_{\text{th}}} + \bar{\mathcal{J}}_{\text{ext}}, \quad (5.78)$$

$$\frac{Z}{\tau} \frac{\delta\bar{n}}{n} = -\frac{2}{\beta_i} \frac{\delta\bar{B}}{B} + (1 - \hat{I}_1)\bar{\varphi} - \frac{1}{n_i} \int d^3\mathbf{v} \hat{v}_{\perp}^2 \hat{J}_1 \bar{g}. \quad (5.79)$$

The external energy-injecting currents are, in fact, supposed to represent energy arriving from much larger scales. It is then a logical choice to set $\bar{\mathcal{J}}_{\text{ext}} = 0$ and treat $\tilde{\mathcal{J}}_{\text{ext}}$ as representing the incoming KAW energy [see (5.84)]. In a similar vein, we shall, in (5.91), let $\tilde{a}_{\text{ext}} = 0$ and treat \bar{a}_{ext} as representing the incoming ICW energy.

5.7.3. Electron Equations

The treatment of the electron equations (3.10) and (3.11) is completely analogous to the treatment of their counterparts (5.14) and (5.15) in section 5.5.3. We retain terms to two leading orders, $\beta_i^{-2/3}$ and $\beta_i^{-1/3}$:

$$\frac{\partial \tilde{\mathcal{A}}}{\partial t} + \frac{v_{\text{th}}}{2} \frac{\partial}{\partial z} \left(\bar{\varphi} - \frac{Z}{\tau} \frac{\delta\tilde{n}}{n} \right) = \frac{v_{\text{th}}}{2} \nabla_{\parallel} \frac{Z}{\tau} \frac{\delta\tilde{n}}{n} + \eta \nabla_{\perp}^2 \tilde{\mathcal{A}}, \quad (5.80)$$

$$\frac{\partial}{\partial t} \left(\frac{\delta\tilde{n}}{n} - \frac{\delta\tilde{B}}{B} \right) + \frac{\partial \bar{u}_{\parallel e}}{\partial z} = -\nabla_{\parallel} \tilde{u}_{\parallel e}, \quad \text{where} \quad \nabla_{\parallel} = \frac{\partial}{\partial z} - \rho_i \{ \tilde{\mathcal{A}}, \dots \}. \quad (5.81)$$

If these are averaged over the KAW time scale and then its average is subtracted from each equation, we obtain, using also (5.75) and (5.76),

$$\frac{\partial \tilde{\mathcal{A}}}{\partial t} = -\frac{v_{\text{th}}}{\beta_i} \widetilde{\nabla_{\parallel} \frac{\delta\tilde{B}}{B}} + \eta \nabla_{\perp}^2 \tilde{\mathcal{A}}, \quad (5.82)$$

$$\frac{\partial}{\partial t} \left(1 + \frac{2}{\beta_e} \right) \frac{\delta\tilde{B}}{B} = v_{\text{th}} \nabla_{\parallel} \left(\frac{1}{\beta_i} \widetilde{\hat{\nabla}_{\perp}^2 \tilde{\mathcal{A}} + \tilde{\mathcal{J}}_{\text{ext}}} \right). \quad (5.83)$$

These are just the KAW equations (5.36) in different notation, but now they are valid at $k_{\perp} \rho_i \sim 1$, i.e., both above and below the Larmor scale. They are entirely decoupled from ion dynamics and so the KAW energy will cascade right through the Larmor scale and eventually dissipate into electron heat.

To restate the last point in terms of a free-energy budget, the system (5.82–5.83) obeys

$$\frac{dW_{\text{KAW}}}{dt} + Q_e = v_{\text{th}}^2 \int \frac{d^3\mathbf{r}}{V} \frac{\partial \tilde{\mathcal{A}}}{\partial t} \tilde{\mathcal{J}}_{\text{ext}} = \varepsilon_{\text{KAW}}, \quad (5.84)$$

²²Note that since we are now using overbars to denote time averages, we have suspended the overbar notation for ion velocity integrals and reverted to writing them explicitly.

where W_{KAW} is given by (5.41) [it is the same as the last two terms of (3.30), after using (5.76)], Q_e is given by (3.21) (with $\mathcal{A} \rightarrow \tilde{\mathcal{A}}$) and $\tilde{\mathcal{J}}_{\text{ext}}$ now represents the KAW cascade from $k_{\perp}\rho_i \ll 1$. In steady state,

$$Q_e = \varepsilon_{\text{KAW}}. \quad (5.85)$$

Returning to the averaged versions of (5.80) and (5.81) and retaining only the lowest order, we find

$$\frac{\partial}{\partial z} \left(\bar{\varphi} - \frac{Z}{\tau} \frac{\delta \bar{n}}{n} \right) = 0, \quad \frac{\partial \bar{u}_{\parallel e}}{\partial z} = 0. \quad (5.86)$$

With the aid of (5.78) and (5.79), these are readily seen to be the $k_{\perp}\rho_i \sim 1$ counterparts of the ICW “constitutive relations” (5.39). When they are written in the form (5.86), their physical meaning becomes particularly transparent: these are statements of Boltzmann (“adiabatic”) electrons and zero electron current, usually associated with the electrostatic approximation. We shall see in section 5.7.4 that ion dynamics on ICW time scales are indeed electrostatic.

5.7.4. Ion Equations

Finally, we treat the ion GK equation (3.29) in the same manner as we did the electron equations in section 5.7.3. To two lowest orders, it is

$$\begin{aligned} \frac{\partial \bar{g}}{\partial t} + \frac{\rho_i v_{\text{th}}}{2} \{ \langle \bar{\varphi} \rangle_{\mathbf{R}}, \bar{g} \} + \frac{\partial}{\partial t} \left(\tilde{g} - \hat{v}_{\perp}^2 \hat{J}_1 \frac{\delta \tilde{B}}{B} F_0 \right) + v_{\parallel} \left\langle \frac{\partial}{\partial z} \left(\bar{g} + \frac{Z}{\tau} \frac{\delta \bar{n}}{n} F_0 \right) + \nabla_{\parallel} \frac{Z}{\tau} \frac{\delta \tilde{n}}{n} F_0 \right\rangle_{\mathbf{R}} \\ = C[\bar{g} + \tilde{g} + \langle \bar{\varphi} + \tilde{\varphi} \rangle_{\mathbf{R}} F_0] + \frac{2v_{\parallel} \langle \bar{a}_{\text{ext}} + \tilde{a}_{\text{ext}} \rangle_{\mathbf{R}}}{v_{\text{th}}^2} F_0. \end{aligned} \quad (5.87)$$

Taking the KAW-time-scale average of (5.87) and then subtracting it from the equation, we get

$$\frac{\partial}{\partial t} \left(\tilde{g} - \hat{v}_{\perp}^2 \hat{J}_1 \frac{\delta \tilde{B}}{B} F_0 \right) = v_{\parallel} \left\langle \nabla_{\parallel} \frac{2}{\beta_i} \frac{\delta \tilde{B}}{B} \right\rangle_{\mathbf{R}} F_0 + C[\tilde{g} + \langle \tilde{\varphi} \rangle_{\mathbf{R}} F_0], \quad (5.88)$$

where we have used also (5.76) and set $\tilde{a}_{\text{ext}} = 0$ as promised at the end of section 5.7.2. This is an (irrelevant) imprint of the KAW turbulence on the ion distribution function—the FLR version of (5.38).²³ Note that there is no phase mixing here, either parallel or perpendicular, so, in a weakly collisional plasma, these small perturbations of the ion distribution function have no means of accessing the collision operator and thermalising.

Returning to the KAW-time-scale average of (5.87), retaining the lowest-order terms and using the first equation in (5.86), we get

$$\frac{\partial \bar{g}}{\partial t} + \frac{\rho_i v_{\text{th}}}{2} \{ \langle \bar{\varphi} \rangle_{\mathbf{R}}, \bar{g} \} + v_{\parallel} \frac{\partial}{\partial z} (\bar{g} + \langle \bar{\varphi} \rangle_{\mathbf{R}} F_0) = C[\bar{g} + \langle \bar{\varphi} \rangle_{\mathbf{R}} F_0] + \frac{2v_{\parallel} \langle \bar{a}_{\text{ext}} \rangle_{\mathbf{R}}}{v_{\text{th}}^2} F_0. \quad (5.89)$$

Together with (5.77), this is a closed system—the standard electrostatic GK equation supporting ion hydrodynamics (5.37) at long scales ($k_{\perp}\rho_i \ll 1$)²⁴ and the ion entropy cascade at sub-Larmor scales (see S09–§7.10 and Schekochihin *et al.* 2008). There is no coupling to any other dynamics and so the ICW energy arriving from $k_{\perp}\rho_i \ll 1$ flows into

²³The first and second equations of (5.38) are recovered by taking the density and parallel-velocity moments, respectively, of (5.88), using, in the case of the density moment, (5.83), and going to the $k_{\perp}\rho_i \ll 1$ limit.

²⁴This is again derived by taking the density and parallel-velocity moments of (5.89).

the ion entropy cascade at $k_{\perp}\rho_i \gg 1$, to become, upon reaching collisional phase-space scales, ion heat.

For the reference of a meticulous reader, the dispersion relation that follows from (5.89) and (5.77) is

$$1 + \zeta \mathcal{Z}(\zeta) = 1 - \frac{1}{\Gamma_0}, \quad \zeta = \frac{\omega}{|k_{\parallel}|v_{\text{th}}}, \quad (5.90)$$

where $\mathcal{Z}(\zeta)$ is the plasma dispersion function (Fried & Conte 1961). When $k_{\perp}\rho_i \ll 1$ and (consequently) $\zeta \gg 1$, the right-hand side of (5.90) is $\approx -k_{\perp}^2\rho_i^2/2$ and the left-hand side is $\approx -1/2\zeta^2$ (the “fluid” limit). The result is the ICW dispersion relation (5.30). When $k_{\perp}\rho_i \sim 1$, we must have $\zeta \sim 1$ and the solutions of (5.90) contain heavy Landau damping on the ions—the linear signature of ion heating.

Finally, the free-energy budget of the system (5.89) and (5.77) is

$$\frac{d}{dt} \frac{v_{\text{th}}^2}{4} \int \frac{d^3\mathbf{r}}{V} \left[\frac{1}{n_i} \int d^3\mathbf{v} \frac{\langle \bar{g}^2 \rangle_{\mathbf{r}}}{F_0} + \bar{\varphi}(1 - \hat{I}_0)\bar{\varphi} \right] + Q_i = \int \frac{d^3\mathbf{r}}{V} \frac{1}{n_i} \int d^3\mathbf{v} \bar{a}_{\text{ext}} \langle v_{\parallel} g \rangle_{\mathbf{r}} = \varepsilon_{\text{ICW}}, \quad (5.91)$$

where Q_i is given by (3.20) (with $h \rightarrow \bar{h}$) and, as promised in section 5.7.2, \bar{a}_{ext} now represents the energy flux into the ICW cascade. In the long-wavelength limit $k_{\perp}\rho_i \ll 1$, the individually conserved piece of free energy appearing in the left-hand side turns into the ICW free energy (5.42) plus the variance of the passive kinetic field \mathcal{G} [see (5.13)]. The difference between (5.91) and the analogous low- β_e equation (4.19) is that the “kinetic-energy” term $\bar{\varphi}(1 - \hat{I}_0)\bar{\varphi}$ has now migrated into the ion-heating balance [cf. (4.27) and (3.30)] (removing also the technical complications associated with Q_x). In steady state, (5.91) tells us that

$$Q_i = \varepsilon_{\text{ICW}}, \quad (5.92)$$

restating again that all the ICW energy goes into ion heating.

6. Discussion

The physics of turbulent heating of low-beta GK plasmas was already summarised and discussed at length in section 2, so we need not repeat that discussion. The headline result is the clean separation between the Alfvénic cascade heating the electrons and the compressive cascade the ions, at low β_i and low β_e (section 4). One practical implication is that it becomes an interesting question, not just in itself, but also for large-scale modelling of, e.g., detectable emission from astrophysical objects (e.g., Ressler *et al.* 2017; Chael *et al.* 2018*b,a*), how any particular type of MHD turbulence present in these objects splits itself into these two cascades—the answer to this question for, e.g., MRI turbulence, is not known, although it can, in principle, be obtained via standard fluid simulations. In the solar wind, the answer is known observationally, if not necessarily understood theoretically: the compressive cascade carries about 10% of the energy (Howes *et al.* 2012; Chen 2016).

Obviously, it must be appreciated that our prediction for the energy partition is only as good as the GK (low-frequency) approximation that has been used to make it. The most developed theoretical scheme that breaks this approximation and provides some significant ion heating is the so called “stochastic heating”, caused by turbulent fluctuations distorting ions’ Larmor orbits (Chandran *et al.* 2010); other possibilities involve various forms of cyclotron heating of the ions (e.g. Gary *et al.* 2005; Kasper *et al.* 2008, 2013; Marsch & Bourouaine 2011; Arzamasskiy *et al.* 2019). Thus, our prediction of ion heating should perhaps be viewed as a lower bound.

Let us discuss very briefly the conditions under which the stochastic heating might take over (a more sophisticated recent take on this topic can be found in [Mallet *et al.* 2018](#)).

6.1. Stochastic Heating

The fraction of the Alfvénic energy flux arriving to the ion Larmor scale that gets converted into ion heat via the stochastic heating mechanism is ([Chandran *et al.* 2010](#))

$$Q_i^{(\text{stoch})} \sim \varepsilon_{\text{AW}} e^{-1/\delta}, \quad \delta \sim \frac{u_{\perp, \rho_i}}{v_{\text{th}i}} \sim \frac{1}{\sqrt{\beta_i}} \frac{\delta B_{\perp, \rho_i}}{B_0} \sim \frac{1}{\sqrt{\beta_i}} \frac{\delta B_{\perp L}}{B_0} \left(\frac{\rho_i}{L}\right)^{1/3}, \quad (6.1)$$

where u_{\perp, ρ_i} and $\delta B_{\perp, \rho_i}$ are the typical velocity and magnetic perturbations at the Larmor scale. The last estimate comes from assuming a $k_{\perp}^{-5/3}$ spectrum of the Alfvénic cascade (replace the exponent 1/3 with 1/4 if you prefer $k_{\perp}^{-3/2}$), to refer δ to the magnetic-field variation $\delta B_{\perp L}$ at the outer scale L . Given L and $\delta B_{\perp L}$, which are independent, system-specific properties, setting $\delta \sim 1$ in (6.1) gives us an estimate of the limitations of both the GK and low-beta limits: indeed, in the ordering of section 4.1, $\delta \sim \epsilon/\sqrt{\beta_i}$, so $\delta \sim 1$ is when these two limits clash. In the solar wind, usually, $\delta B_{\perp L}/B_0 \sim 1$ and $\rho_i/L \sim 10^{-4}$, so, if we were to err on the side of caution, we would start disbelieving the GK predictions for $\beta_i \lesssim 10^{-2}$, although it is not hard to play with numbers and lower this by another factor of 10 in specific circumstances. More careful estimates of the validity of the GK approximation can be found in [Howes *et al.* \(2008a\)](#) and of the importance of stochastic heating in [Chandran *et al.* \(2010\)](#) and [Chandran \(2010\)](#). Our purpose here is to emphasise that the constraints that we have placed on the ion heating are pessimistic (from the ions' viewpoint) and may become unreliable when β_i is too low.²⁵

An interesting corollary is that there might be an intrinsic mechanism that would prevent β_i from being much lower than the stochastic-heating threshold: indeed, if β_i did drop lower, stochastic heating would become significant and channel turbulent energy into ions, which would increase β_i and shut down stochastic heating. One could imagine some equilibrium hovering around that threshold in a system where ions, starved of heating in the GK approximation, were able to cool down and thus lower β_i until stochastic heating turned on.

It is perhaps useful to mention two other plausible self-regulation mechanisms implied by our considerations above.

6.2. Energy Redistribution in the Hall Regime

At the price of the rather long derivation in section 5, we learned that the clean energy partition that holds at low β_e breaks down at $\beta_e \gtrsim 1$. If, in a given low- β_i system, electrons are heated preferentially and if that preferential heating leads to electron temperature increasing, then the system will be nudged towards the Hall limit.²⁶ Once $T_i/T_e \sim \beta_i$ (equivalently, $\beta_e \sim 1$), electrons will have to start sharing turbulent energy with ions, probably equally (section 5.5.4). This may mean, effectively, that T_i/T_e cannot decrease further and/or that β_i will be pushed up. Thus, low- β_i plasma is intrinsically averse to electrons getting too hot.

²⁵Note the recent observational analysis by [Vech *et al.* \(2017\)](#) and theoretical arguments by [Mallet *et al.* \(2018\)](#) and [Hoppock *et al.* \(2018\)](#), which suggest that stochastic heating may, quantitatively, be more important, at higher values of β_i , than previously believed.

²⁶If T_e does not change, changing T_i alone cannot, obviously, alter the relative size of $\tau = T_i/T_e$ and β_i because both parameters are $\propto T_i$.

6.3. Collisional Heating

In all of the above (and, in particular, in section 4.5), we have assumed that ion collisions are sufficiently infrequent for the collision operator to become important only at sub-Larmor scales. If, however, ions are starved of heating and are, as a result, cooled by some competing mechanism, their collision frequency will increase. The typical rate at which collisional heating happens is [cf. (4.22)] $\tau_\nu^{-1} \sim \nu_{ii}(k_\perp \rho_i)^2$. This is to be compared with the turbulent-cascade rate: for Alfvénic turbulence, $\tau_{\text{nl}}^{-1} \sim k_\perp u_\perp \sim \varepsilon_{\text{AW}}^{1/3} k_\perp^{2/3}$. Balancing the two rates gives us a “Kolmogorov scale”

$$\tau_\nu^{-1} \sim \tau_{\text{nl}}^{-1} \quad \Rightarrow \quad k_{\perp\nu} \rho_i \sim \frac{\varepsilon_{\text{AW}}^{1/4}}{\rho_i^{1/2} \nu_{ii}^{3/4}} \propto \varepsilon_{\text{AW}}^{1/4} n_i^{-3/4} B^{1/2} T_i^{7/8}. \quad (6.2)$$

If T_i is so low that $k_{\perp\nu} \rho_i \lesssim 1$, the cascade will be dissipated by ion (perpendicular) viscosity and ion heating will result. Again, one can imagine an equilibrium hovering around the transition between the two regimes—collisional and collisionless.

While it is not our purpose here to propose macroscopic thermodynamic models of any specific object, we hope that we have given a more object-oriented reader some food for thought and perhaps even some useful information, while a fellow kinetic-theory enthusiast might have enjoyed the ride. Some of the ideas, loose ends and opportunities for numerical verification identified above will be picked up in our own future work.

We are indebted to W. Dorland, T. Adkins, S. Balbus, S. Cowley, N. Loureiro, F. Parra, and E. Quataert for many important conversations, to B. Chandran, G. Howes and M. Kunz for detailed comments on the draft manuscript, and to R. Meyrand for a tutorial on Hall MHD. The work of YK was supported in full and of MAB and AAS in part by the UK STFC Consolidated Grant ST/N000919/1; AAS was also supported in part by the UK EPSRC Grant EP/M022331/1 and, at NBIA, by the Simons Foundation. The authors are grateful to the Wolfgang Pauli Institute, Vienna, for its hospitality and the scientific interactions that it enabled, on multiple occasions.

REFERENCES

- ABEL, I. G., BARNES, M., COWLEY, S. C., DORLAND, W. & SCHEKOCIHIN, A. A. 2008 Linearized model Fokker-Planck collision operators for gyrokinetic simulations. I. Theory. *Phys. Plasmas* **15**, 122509.
- ABEL, I. G., PLUNK, G. G., WANG, E., BARNES, M., COWLEY, S. C., DORLAND, W. & SCHEKOCIHIN, A. A. 2013 Multiscale gyrokinetics for rotating tokamak plasmas: fluctuations, transport and energy flows. *Rep. Prog. Phys.* **76**, 116201.
- ALEXandroVA, O., SAUR, J., LACOMBE, C., MANGENEY, A., MITCHELL, J., SCHWARTZ, S. J. & ROBERT, P. 2009 Universality of solar-wind turbulent spectrum from MHD to electron scales. *Phys. Rev. Lett.* **103**, 165003.
- ARZAMASSKIY, L., KUNZ, M. W., CHANDRAN, B. D. G. & QUATAERT, E. 2019 Hybrid-kinetic simulations of ion heating in Alfvénic turbulence. *E-print arXiv:1901.11028*.
- ASCHWANDEN, M. J., POLAND, A. I. & RABIN, D. M. 2001 The new solar corona. *Annu. Rev. Astron. Astrophys.* **39**, 175.
- BAÑÓN NAVARRO, A., TEACA, B., TOLD, D., GROŠELJ, D., CRANDALL, P. & JENKO, F. 2016 Structure of plasma heating in gyrokinetic Alfvénic turbulence. *Phys. Rev. Lett.* **117**, 245101.
- BALE, S. D., KASPER, J. C., HOWES, G. G., QUATAERT, E., SALEM, C. & SUNDKVIST, D. 2009 Magnetic fluctuation power near proton temperature anisotropy instability thresholds in the solar wind. *Phys. Rev. Lett.* **103**, 211101.

- BANERJEE, S. & GALTIER, S. 2016 Chiral exact relations for helicities in Hall magnetohydrodynamic turbulence. *Phys. Rev. E* **93**, 033120.
- BARNES, A. 1966 Collisionless damping of hydromagnetic waves. *Phys. Fluids* **9**, 1483.
- BELL, N. & NAZARENKO, S. 2019 Rotating magnetohydrodynamic turbulence. *E-print arXiv:1902.07524*.
- BIAN, N. H. & TSIKLARI, D. 2009 Compressible Hall magnetohydrodynamics in a strong magnetic field. *Phys. Plasmas* **16**, 064503.
- BOLDYREV, S., HORAITES, K., XIA, Q. & PEREZ, J. C. 2013 Toward a theory of astrophysical plasma turbulence at subproton scales. *Astrophys. J.* **777**, 41.
- BOLDYREV, S. & LOUREIRO, N. F. 2019 Role of reconnection in inertial kinetic-Alfvén turbulence. *E-print arXiv:1901.10096*.
- BOLDYREV, S. & PEREZ, J. C. 2012 Spectrum of kinetic-Alfvén turbulence. *Astrophys. J.* **758**, L44.
- BOOZER, A. H. 2018 Why fast magnetic reconnection is so prevalent. *J. Plasma Phys.* **84**, 715840102.
- BRAGINSKII, S. I. 1965 Transport processes in a plasma. *Rev. Plasma Phys.* **1**, 205.
- BREECH, B., MATTHAEUS, W. H., CRANMER, S. R., KASPER, J. C. & OUGHTON, S. 2009 Electron and proton heating by solar wind turbulence. *J. Geophys. Res.* **114**, A09103.
- CARTER, T. A., BRUGMAN, B., PRIBYL, P. & LYBARGER, W. 2006 Laboratory observation of a nonlinear interaction between shear Alfvén waves. *Phys. Rev. Lett.* **96**, 155001.
- CERRI, S. S., KUNZ, M. W. & CALIFANO, F. 2018 Dual phase-space cascades in 3D hybrid-Vlasov-Maxwell turbulence. *Astrophys. J.* **856**, L13.
- CHAE, A., NARAYAN, R. & JOHNSON, M. D. 2018a Two-temperature, magnetically arrested disc simulations of the jet from the supermassive black hole in M87. *E-print arXiv:1810.01983*.
- CHAE, A., ROWAN, M., NARAYAN, R., JOHNSON, M. & SIRONI, L. 2018b The role of electron heating physics in images and variability of the Galactic Centre black hole Sagittarius A*. *Mon. Not. R. Astron. Soc.* **478**, 5209.
- CHANDRAN, B. D. G. 2010 Alfvén-wave turbulence and perpendicular ion temperatures in coronal holes. *Astrophys. J.* **720**, 548.
- CHANDRAN, B. D. G., FOUCART, F. & TCHEKHOVSKOY, A. 2018 Heating of accretion-disk coronae and jets by general relativistic magnetohydrodynamic turbulence. *J. Plasma Phys.* **84**, 905840310.
- CHANDRAN, B. D. G., LI, B., ROGERS, B. N., QUATAERT, E. & GERMASCHEWSKI, K. 2010 Perpendicular ion heating by low-frequency Alfvén-wave turbulence in the solar wind. *Astrophys. J.* **720**, 503.
- CHANDRAN, B. D. G., QUATAERT, E., HOWES, G. G., XIA, Q. & PONGKITIWANICHAKUL, P. 2009 Constraining low-frequency Alfvénic turbulence in the solar wind using density-fluctuation measurements. *Astrophys. J.* **707**, 1668.
- CHASTON, C. C., SALEM, C., BONNELL, J. W., CARLSON, C. W., ERGUN, R. E., STRANGEWAY, R. J. & MCFADDEN, J. P. 2008 The turbulent Alfvénic aurora. *Phys. Rev. Lett.* **100**, 175003.
- CHEN, C. H. K. 2016 Recent progress in astrophysical plasma turbulence from solar wind observations. *J. Plasma Phys.* **82**, 535820602.
- CHEN, C. H. K. & BOLDYREV, S. 2017 Nature of kinetic scale turbulence in the Earth's magnetosheath. *Astrophys. J.* **842**, 122.
- CHEN, C. H. K., BOLDYREV, S., XIA, Q. & PEREZ, J. C. 2013 Nature of subproton scale turbulence in the solar wind. *Phys. Rev. Lett.* **110**, 225002.
- CHEN, C. H. K., MALLET, A., YOUSEF, T. A., SCHEKOCIHIN, A. A. & HORBURY, T. S. 2011 Anisotropy of Alfvénic turbulence in the solar wind and numerical simulations. *Mon. Not. R. Astron. Soc.* **415**, 3219.
- CHEN, Q., CHEN, S. & EYINK, G. L. 2003 The joint cascade of energy and helicity in three-dimensional turbulence. *Phys. Fluids* **15**, 361.
- CHO, J. & KIM, H. 2016 Spectral evolution of helical electron magnetohydrodynamic turbulence. *J. Geophys. Res. A* **121**, 6157.
- CHO, J. & LAZARIAN, A. 2004 The anisotropy of electron magnetohydrodynamic turbulence. *Astrophys. J.* **615**, L41.

- CHO, J. & LAZARIAN, A. 2009 Simulations of electron magnetohydrodynamic turbulence. *Astrophys. J.* **701**, 236.
- CHO, J. & VISHNIAC, E. T. 2000 The anisotropy of magnetohydrodynamic Alfvénic turbulence. *Astrophys. J.* **539**, 273–282.
- CRANMER, S. R. 2009 Coronal holes. *Living Rev. Solar Phys.* **6**, 3.
- CRANMER, S. R., MATTHAEUS, W. H., BREECH, B. A. & KASPER, J. C. 2009 Empirical constraints on proton and electron heating in the fast solar wind. *Astrophys. J.* **702**, 1604.
- DAVIDSON, P. A. 2013 *Turbulence in Rotating, Stratified and Electrically Conducting Fluids*. Cambridge: Cambridge University Press.
- EYINK, G. L. 2015 Turbulent general magnetic reconnection. *Astrophys. J.* **807**, 137.
- EYINK, G. L. 2018 Cascades and dissipative anomalies in nearly collisionless plasma turbulence. *Phys. Rev. X* **8**, 041020.
- FRANCI, L., LANDI, S., VERDINI, A., MATTEINI, L. & HELLINGER, P. 2018 Solar wind turbulent cascade from MHD to sub-ion scales: large-size 3D hybrid particle-in-cell simulations. *Astrophys. J.* **853**, 26.
- FRIED, B. D. & CONTE, S. D. 1961 *The Plasma Dispersion Function*. New York: Academic Press.
- FRIEMAN, E. A. & CHEN, L. 1982 Nonlinear gyrokinetic equations for low-frequency electromagnetic waves in general plasma equilibria. *Phys. Fluids* **25**, 502.
- GALTIER, S. 2014 Weak turbulence theory for rotating magnetohydrodynamics and planetary flows. *J. Fluid Mech.* **757**, 114.
- GALTIER, S. & BUCHLIN, E. 2007 Multiscale Hall-magnetohydrodynamic turbulence in the solar wind. *Astrophys. J.* **656**, 560.
- GARY, S. P., SMITH, C. W. & SKOUG, R. M. 2005 Signatures of Alfvén-cyclotron wave-ion scattering: Advanced Composition Explorer (ACE) solar wind observations. *J. Geophys. Res.* **110**, A07108.
- GEKELMAN, W., VINCENA, S., VAN COMPERNOLLE, B., MORALES, G. J., MAGGS, J. E., PRIBYL, P. & CARTER, T. A. 2011 The many faces of shear Alfvén waves. *Phys. Plasmas* **18**, 055501.
- GOLDREICH, P. & SRIDHAR, S. 1995 Toward a theory of interstellar turbulence. 2: Strong Alfvénic turbulence. *Astrophys. J.* **438**, 763.
- GOLDREICH, P. & SRIDHAR, S. 1997 Magnetohydrodynamic turbulence revisited. *Astrophys. J.* **485**, 680.
- GÓMEZ, D. O., MAHAJAN, S. M. & DMITRUK, P. 2008 Hall magnetohydrodynamics in a strong magnetic field. *Phys. Plasmas* **15**, 102303.
- GROŠELJ, D., CERRI, S. S., BAÑÓN NAVARRO, A., WILLMOTT, C., TOLD, D., LOUREIRO, N. F., CALIFANO, F. & JENKO, F. 2017 Fully kinetic versus reduced-kinetic modeling of collisionless plasma turbulence. *Astrophys. J.* **847**, 28.
- GROŠELJ, D., MALLET, A., LOUREIRO, N. F. & JENKO, F. 2018 Fully kinetic simulation of 3D kinetic Alfvén turbulence. *Phys. Rev. Lett.* **120**, 105101.
- HE, J., MARSCH, E., TU, C., YAO, S. & TIAN, H. 2011 Possible evidence of Alfvén-cyclotron waves in the angle distribution of magnetic helicity of solar wind turbulence. *Astrophys. J.* **731**, 85.
- HE, J., TU, C., MARSCH, E. & YAO, S. 2012 Reproduction of the observed two-component magnetic helicity in solar wind turbulence by a superposition of parallel and oblique Alfvén waves. *Astrophys. J.* **749**, 86.
- HELANDER, P. & SIGMAR, D. J. 2005 *Collisional Transport in Magnetized Plasmas*. Cambridge: Cambridge University Press.
- HELLINGER, P., TRÁVNÍČEK, P., KASPER, J. C. & LAZARUS, A. J. 2006 Solar wind proton temperature anisotropy: Linear theory and WIND/SWE observations. *Geophys. Res. Lett.* **33**, L09101.
- HOPPOCK, I. W., CHANDRAN, B. D. G., KLEIN, K. G., MALLET, A. & VERSCHAREN, D. 2018 Stochastic proton heating by kinetic-Alfvén-wave turbulence in moderately high- β plasmas. *J. Plasma Phys.* **84**, 905840615.
- HORBURY, T. S., FORMAN, M. & OUGHTON, S. 2008 Anisotropic scaling of magnetohydrodynamic turbulence. *Phys. Rev. Lett.* **101**, 175005.

- HOWES, G. G. 2010 A prescription for the turbulent heating of astrophysical plasmas. *Mon. Not. R. Astron. Soc.* **409**, L104.
- HOWES, G. G. 2011 Prediction of the proton-to-total turbulent heating in the solar wind. *Astrophys. J.* **738**, 40.
- HOWES, G. G. 2015 The inherently three-dimensional nature of magnetized plasma turbulence. *J. Plasma Phys.* **81**, 325810203.
- HOWES, G. G., BALE, S. D., KLEIN, K. G., CHEN, C. H. K., SALEM, C. S. & TENBARGE, J. M. 2012 The slow-mode nature of compressible wave power in solar wind turbulence. *Astrophys. J.* **753**, L19.
- HOWES, G. G., COWLEY, S. C., DORLAND, W., HAMMETT, G. W., QUATAERT, E. & SCHEKOCHIHIN, A. A. 2006 Astrophysical gyrokinetics: basic equations and linear theory. *Astrophys. J.* **651**, 590.
- HOWES, G. G., COWLEY, S. C., DORLAND, W., HAMMETT, G. W., QUATAERT, E. & SCHEKOCHIHIN, A. A. 2008a A model of turbulence in magnetized plasmas: implications for the dissipation range in the solar wind. *J. Geophys. Res.* **113**, A05103.
- HOWES, G. G., DORLAND, W., COWLEY, S. C., HAMMETT, G. W., QUATAERT, E., SCHEKOCHIHIN, A. A. & TATSUNO, T. 2008b Kinetic simulations of magnetized turbulence in astrophysical plasmas. *Phys. Rev. Lett.* **100**, 065004.
- HOWES, G. G., TENBARGE, J. M., DORLAND, W., QUATAERT, E., SCHEKOCHIHIN, A. A., NUMATA, R. & TATSUNO, T. 2011 Gyrokinetic simulations of solar wind turbulence from ion to electron scales. *Phys. Rev. Lett.* **107**, 035004.
- KADOMTSEV, B. B. & POGUTSE, O. P. 1974 Nonlinear helical perturbations of a plasma in the tokamak. *Soviet Phys. JETP* **38**, 283.
- KASPER, J. C., LAZARUS, A. J. & GARY, S. P. 2008 Hot solar-wind helium: direct evidence for local heating by Alfvén-cyclotron dissipation. *Phys. Rev. Lett.* **101**, 261103.
- KASPER, J. C., MARUCA, B. A., STEVENS, M. L. & ZASLAVSKY, A. 2013 Sensitive test for ion-cyclotron resonant heating in the solar wind. *Phys. Rev. Lett.* **110**, 091102.
- KAWAZURA, Y. & BARNES, M. 2018 A hybrid gyrokinetic ion and isothermal electron fluid code for astrophysical plasma. *J. Comp. Phys.* **360**, 57.
- KAWAZURA, Y., BARNES, M. & SCHEKOCHIHIN, A. A. 2019 Thermal disequilibrium of ions and electrons by collisionless plasma turbulence. *Proc. Nat. Acad. Sci.* **116**, 771.
- KLEIN, K. G., HOWES, G. G., TENBARGE, J. M. & PODESTA, J. J. 2014 Physical interpretation of the angle-dependent magnetic helicity spectrum in the solar wind: the nature of turbulent fluctuations near the proton gyroradius scale. *Astrophys. J.* **785**, 138.
- KRISHAN, V. & MAHAJAN, S. M. 2004 Magnetic fluctuations and Hall magnetohydrodynamic turbulence in the solar wind. *J. Geophys. Res.* **109**, A11105.
- KUNZ, M. W., ABEL, I. G., KLEIN, K. G. & SCHEKOCHIHIN, A. A. 2018 Astrophysical gyrokinetics: turbulence in pressure-anisotropic plasmas at ion scales and beyond. *J. Plasma Phys.* **84**, 715840201.
- KUNZ, M. W., SCHEKOCHIHIN, A. A., CHEN, C. H. K., ABEL, I. G. & COWLEY, S. C. 2015 Inertial-range kinetic turbulence in pressure-anisotropic astrophysical plasmas. *J. Plasma Phys.* **81**, 325810501.
- LI, T. C., HOWES, G. G., KLEIN, K. G. & TENBARGE, J. M. 2016 Energy dissipation and Landau damping in two- and three-dimensional plasma turbulence. *Astrophys. J.* **832**, L24.
- LION, S., ALEXANDROVA, O. & ZASLAVSKY, A. 2016 Coherent events and spectral shape at ion kinetic scales in the fast solar wind turbulence. *Astrophys. J.* **824**, 47.
- LITHWICK, Y. & GOLDREICH, P. 2001 Compressible magnetohydrodynamic turbulence in interstellar plasmas. *Astrophys. J.* **562**, 279.
- LOUREIRO, N. F. & BOLDYREV, S. 2017 Collisionless reconnection in magnetohydrodynamic and kinetic turbulence. *Astrophys. J.* **850**, 182.
- LOUREIRO, N. F., DORLAND, W., FAZENDEIRO, L., KANEKAR, A., MALLET, A., VILELAS, M. S. & ZOCCO, A. 2016 Viriato: A Fourier-Hermite spectral code for strongly magnetized fluid-kinetic plasma dynamics. *Comp. Phys. Comm.* **206**, 45.
- LOUREIRO, N. F., SCHEKOCHIHIN, A. A. & ZOCCO, A. 2013 Fast collisionless reconnection and electron heating in strongly magnetized plasmas. *Phys. Rev. Lett.* **111**, 025002.

- MAHAJAN, S. M. & YOSHIDA, Z. 1998 Double curl Beltrami flow: diamagnetic structures. *Phys. Rev. Lett.* **81**, 4863.
- MALLET, A., KLEIN, K. G., CHANDRAN, B. D. G., GROŠELJ, D., HOPPOCK, I. W., BOWEN, T. A., SALEM, C. S. & BALE, S. D. 2018 Interplay between intermittency and dissipation in collisionless plasma turbulence. *E-print* arXiv:1807.09301.
- MARON, J. & GOLDREICH, P. 2001 Simulations of incompressible magnetohydrodynamic turbulence. *Astrophys. J.* **554**, 1175.
- MARSCH, E. & BOUROUAINE, S. 2011 Velocity-space diffusion of solar wind protons in oblique waves and weak turbulence. *Ann. Geophys.* **29**, 2089.
- MEYRAND, R. & GALTIER, S. 2012 Spontaneous chiral symmetry breaking of Hall magnetohydrodynamic turbulence. *Phys. Rev. Lett.* **109**, 194501.
- MEYRAND, R. & GALTIER, S. 2013 Anomalous $k_{\perp}^{-8/3}$ spectrum in electron magnetohydrodynamic turbulence. *Phys. Rev. Lett.* **111**, 264501.
- MEYRAND, R., KANEKAR, A., DORLAND, W. & SCHEKOCIHIN, A. A. 2019 Fluidization of collisionless plasma turbulence. *Proc. Nat. Acad. Sci.* **116**, 1185.
- MEYRAND, R., KIYANI, K. H., GÜRCAN, Ö. D. & GALTIER, S. 2018 Coexistence of weak and strong wave turbulence in incompressible Hall magnetohydrodynamics. *Phys. Rev. X* **8**, 031066.
- NAZARENKO, S. V. & SCHEKOCIHIN, A. A. 2011 Critical balance in magnetohydrodynamic, rotating and stratified turbulence: towards a universal scaling conjecture. *J. Fluid Mech.* **677**, 134.
- PASSOT, T., SULEM, P. L. & TASSI, E. 2017 Electron-scale reduced fluid models with gyroviscous effects. *J. Plasma Phys.* **83**, 715830402.
- PLUNK, G. G., COWLEY, S. C., SCHEKOCIHIN, A. A. & TATSUNO, T. 2010 Two-dimensional gyrokinetic turbulence. *J. Fluid Mech.* **664**, 407.
- PODESTA, J. J. 2009 Dependence of solar-wind power spectra on the direction of the local mean magnetic field. *Astrophys. J.* **698**, 986.
- PODESTA, J. J. & GARY, S. P. 2011 Magnetic helicity spectrum of solar wind fluctuations as a function of the angle with respect to the local mean magnetic field. *Astrophys. J.* **734**, 15.
- QUATAERT, E. 1998 Particle heating by Alfvénic turbulence in hot accretion flows. *Astrophys. J.* **500**, 978.
- QUATAERT, E. 2003 Radiatively inefficient accretion flow models of Sgr A*. *Astron. Nachr.* **324**, 435.
- QUATAERT, E. & GRUZINOV, A. 1999 Turbulence and particle heating in advection-dominated accretion flows. *Astrophys. J.* **520**, 248.
- RESSLER, S. M., TCHEKHOVSKOY, A., QUATAERT, E. & GAMMIE, C. F. 2017 The disc-jet symbiosis emerges: modelling the emission of Sagittarius A* with electron thermodynamics. *Mon. Not. R. Astron. Soc.* **467**, 3604.
- ROWAN, M. E., SIRONI, L. & NARAYAN, R. 2017 Electron and proton heating in transrelativistic magnetic reconnection. *Astrophys. J.* **850**, 29.
- ROWAN, M. E., SIRONI, L. & NARAYAN, R. 2019 Electron and proton heating in transrelativistic guide field reconnection. *E-print* arXiv:1901.05438.
- SAHRAOUI, F., GALTIER, S. & BELMONT, G. 2007 On waves in incompressible Hall magnetohydrodynamics. *J. Plasma Phys.* **73**, 723.
- SAHRAOUI, F., GOLDSTEIN, M. L., BELMONT, G., CANU, P. & REZEAU, L. 2010 Three dimensional anisotropic k spectra of turbulence at subproton scales in the solar wind. *Phys. Rev. Lett.* **105**, 131101.
- SALEM, C. S., HOWES, G. G., SUNDKVIST, D., BALE, S. D., CHASTON, C. C., CHEN, C. H. K. & MOZER, F. S. 2012 Identification of kinetic Alfvén wave turbulence in the solar wind. *Astrophys. J.* **745**, L9.
- SCHEKOCIHIN, A. A., COWLEY, S. C., DORLAND, W., HAMMETT, G. W., HOWES, G. G., PLUNK, G. G., QUATAERT, E. & TATSUNO, T. 2008 Gyrokinetic turbulence: a nonlinear route to dissipation through phase space. *Plasma Phys. Control. Fusion* **50**, 124024.
- SCHEKOCIHIN, A. A., COWLEY, S. C., DORLAND, W., HAMMETT, G. W., HOWES, G. G., QUATAERT, E. & TATSUNO, T. 2009 Astrophysical gyrokinetics: kinetic and fluid

- turbulent cascades in magnetized weakly collisional plasmas. *Astrophys. J. Suppl.* **182**, 310.
- SCHEKOCHIHIN, A. A., PARKER, J. T., HIGHCOCK, E. G., DELLAR, P. J., DORLAND, W. & HAMMETT, G. W. 2016 Phase mixing versus nonlinear advection in drift-kinetic plasma turbulence. *J. Plasma Phys.* **82**, 905820212.
- SHARMA, P., QUATAERT, E., HAMMETT, G. W. & STONE, J. M. 2007 Electron heating in hot accretion flows. *Astrophys. J.* **667**, 714.
- SMITH, C. W., MULLAN, D. J., NESS, N. F., SKOUG, R. M. & STEINBERG, J. 2001 Day the solar wind almost disappeared: Magnetic field fluctuations, wave refraction and dissipation. *J. Geophys. Res.* **106**, 18625.
- STRAUSS, H. R. 1976 Nonlinear, three-dimensional magnetohydrodynamics of noncircular tokamaks. *Phys. Fluids* **19**, 134.
- TATSUNO, T., DORLAND, W., SCHEKOCHIHIN, A. A., PLUNK, G. G., BARNES, M., COWLEY, S. C. & HOWES, G. G. 2009 Nonlinear phase mixing and phase-space cascade of entropy in gyrokinetic plasma turbulence. *Phys. Rev. Lett.* **103**, 015003.
- TENBARGE, J. M. & HOWES, G. G. 2012 Evidence of critical balance in kinetic Alfvén wave turbulence simulations. *Phys. Plasmas* **19**, 055901.
- TENBARGE, J. M., HOWES, G. G. & DORLAND, W. 2013 Collisionless damping at electron scales in solar wind turbulence. *Astrophys. J.* **774**, 139.
- TENBARGE, J. M., HOWES, G. G., DORLAND, W. & HAMMETT, G. W. 2014 An oscillating Langevin antenna for driving plasma turbulence simulations. *Comp. Phys. Comm.* **185**, 578.
- TOLD, D., JENKO, F., TENBARGE, J. M., HOWES, G. G. & HAMMETT, G. W. 2015 Multiscale nature of the dissipation range in gyrokinetic simulations of Alfvénic turbulence. *Phys. Rev. Lett.* **115**, 025003.
- TURNER, L. 1986 Hall effects on magnetic relaxation. *IEEE Trans. Plasma Sci.* **14**, 849.
- VECH, D., KLEIN, K. G. & KASPER, J. C. 2017 Nature of stochastic ion heating in the solar wind: testing the dependence on plasma beta and turbulence amplitude. *Astrophys. J.* **850**, L11.
- WICKS, R. T., HORBURY, T. S., CHEN, C. H. K. & SCHEKOCHIHIN, A. A. 2010 Power and spectral index anisotropy of the entire inertial range of turbulence in the fast solar wind. *Mon. Not. R. Astron. Soc.* **407**, L31.
- XU, R. & KUNZ, M. W. 2016 Linear Vlasov theory of a magnetised, thermally stratified atmosphere. *J. Plasma Phys.* **82**, 905820507.
- ZEMAN, O. 1994 A note on the spectra and decay of rotating homogeneous turbulence. *Phys. Fluids* **6**, 3221.
- ZHDANKIN, V., UZDENSKY, D. A., WERNER, G. R. & BEGELMAN, M. C. 2019 Electron and ion energization in relativistic plasma turbulence. *Phys. Rev. Lett.* **122**, 055101.
- ZOCCO, A. & SCHEKOCHIHIN, A. A. 2011 Reduced fluid-kinetic equations for low-frequency dynamics, magnetic reconnection, and electron heating in low-beta plasmas. *Phys. Plasmas* **18**, 102309.